NASA TM X-74

TECHNICAL MEMORANDUM

TRANSONIC WIND-TUNNEL INVESTIGATION OF

NOZZLE HINGE MOMENTS FOR A LARGE BALLISTIC MISSILE

HAVING TWO GIMBALED ROCKET MOTORS

By James W. Schmeer, Conrad M. Willis,
and Edwin E. Lee, Jr.

Langley Research Center
Langley Field, Va.

NATIONAL AERONAUTICS AND SPACE ADMINISTRATION

WASHINGTON

November 1959

NATIONAL AERONAUTICS AND SPACE ADMINISTRATION

TECHNICAL MEMORANDUM X-74

TRANSONIC WIND-TUNNEL INVESTIGATION OF NOZZLE HINGE MOMENTS FOR A LARGE BALLISTIC MISSILE HAVING TWO GIMBALED ROCKET MOTORS*

By James W. Schmeer, Conrad M. Willis,
and Edwin E. Lee, Jr.

SUMMARY

An investigation of nozzle hinge moments on a large ballistic missile having two gimbaled rocket motors has been conducted in the Langley 16-foot transonic tunnel. Jet-off and jet-on data were obtained through an angle-of-attack range for Mach numbers from 0.80 to 1.10 at an average Reynolds number of 4×10^6 per foot. The effects of jet static-pressure ratio, nozzle deflection, skirt length, and skirt venting (longitudinal slots) were investigated. The flow about the base was briefly studied by means of flow visualization, base pressures, and base temperatures.

The results indicate that nozzle hinge moments are a function of external-flow impingement and base pressures and are dependent on boundary-layer conditions at the model base. Decreasing skirt length, increasing nozzle deflection, and either increasing or decreasing angle of attack from 0° increases hinge moments. Jet exhaust greatly increases hinge moments at low pressure ratios, but the effect decreases with increasing pressure ratio. Venting the skirt generally increased jet-off hinge moments, except at a Mach number of 1.10, but decreased jet-on hinge moments with the greatest reduction occurring at a Mach number of 1.10. Slots also reduced the recirculation of jet exhaust into the base.

INTRODUCTION

Some of the current large ballistic missiles derive directional stability and control from gimbaled rocket motors. In the design of

*Title, Unclassified.

the actuator systems for these controls, calculations of the torque loads due to inertial and frictional forces can be made readily; but, generally the loads due to aerodynamic forces must be obtained experimentally.

At the present time there are little data available for use in the design of missile control systems using gimbaled rocket motors. Therefore, the primary purpose of the present investigation made in the Langley 16-foot transonic tunnel was to obtain nozzle hinge-moment data, including the effects of a hot-jet exhaust, for a large ballistic missile having two gimbaled rocket motors. A secondary purpose was to investigate briefly the flow at the base of the model by means of flow-visualization studies, base-pressure measurements, and base-temperature measurements. Reference 1 presents some jet-off nozzle hinge moments and base-flow studies for a missile with two rocket motors; reference 2 presents some information concerning the base-flow problem for a single hot propulsive jet.

The Mach number range of the present tests was from 0.80 to 1.10 at an average Reynolds number of about 4×10^6 per foot. In this speed range the dynamic pressure, and thus the aerodynamic loads, would be near maximum for a typical flight program of a large missile.

Jet-off data were obtained at angles of attack and angles of sideslip from about -9.5° to 5° with nozzle deflections from -8.7° to 0.2° in the pitch plane and from -2.8° to 6.2° in the yaw plane. Jet-on data were obtained at a reduced number of test conditions which were considered to be sufficient to evaluate the jet effects. Jet static-pressure ratios ranged from about 1.5 to 2.4 which is typical of large missiles in the speed range of this investigation.

SYMBOLS

A	area
C_h	hinge-moment coefficient, M_h/qd^3 (see fig. 3 for sign convention)
C_p	pressure coefficient, $p_l - p_\infty/q$
D	diameter of model base
d	diameter of rocket nozzle exit
H_2O_2	hydrogen peroxide
h	distance from model surface, positive outward

l	length
M	Mach number
M_h	nozzle hinge moment about gimbal axis
p	static pressure
p_t	total pressure
q	dynamic pressure
R	center-body ordinate, radial distance from nozzle axis
r	radius
T	total temperature
ΔT	temperature increment, $T_{on} - T_{off}$
x	distance from nozzle exit, positive forward
y	radial distance from nozzle axis
α	angle of attack
β	angle of sideslip
δ	nozzle deflection angle in lateral plane (see fig. 3 for sign convention)
θ	upper nozzle deflection angle in pitch plane (see fig. 3 for sign convention)
ϕ	meridian angle (see fig. 2)

Subscripts:

b	base
e	jet exit
j	jet
L	lateral plane
l	local

on	rockets operating
off	rockets not operating
V	vertical or pitch plane
∞	free stream

APPARATUS AND METHODS

Tunnel and Jet-Simulator System

The investigation was conducted in the Langley 16-foot transonic tunnel which is described in reference 3.

A hot-jet exhaust was obtained from the catalytic decomposition of hydrogen peroxide (H_2O_2) by means of a bed of silver screens. The jet decomposition temperature of H_2O_2 with a concentration of 90 percent by weight is about 1,365° F and the ratio of specific heat is 1.27. The chamber-pressure range for the tunnel tests was from 26 to 53 pounds per square inch. A complete description of the jet-simulator system used in these tests is given in reference 4.

Model

Basic model and support system.- The model used in this investigation simulated a two-stage ballistic missile having a blunt nose and cylindrical first and second stages connected by a conical transition section. Two first-stage rocket simulators were mounted in gimbals at the base of the model. The model was supported by a 45° sweptback strut with a thickness-chord ratio of 0.05 parallel to the body axis. The strut was an integral part of a tapered sting which was attached to the model support system through a -5° knuckle. At zero angle of attack the model axis was 15 inches above the tunnel center line. A photograph of the basic model mounted in the 16-foot tunnel is shown in figure 1, and a dimensional sketch of the model is shown in figure 2. Also shown in figure 2 is a short model, that is, the model with a shortened second stage. The purpose of the short-length model was to reduce the effects of shock reflections at supersonic speeds as will be discussed in a subsequent section titled "Tests." Figure 3 shows the sign convention used for the nozzle deflection and hinge moments.

Skirt configurations.- Figure 2 shows dimensional sketches of several skirt configurations including skirts of different lengths and

one with 12 longitudinal slots designed to alleviate the recirculation problem, that is, the entrainment of hot fuel-rich exhaust gases into the missile base. A photograph of the slotted skirt is shown in figure 4.

Nozzles.- Shown in the photographs of figure 5 are two sets of rocket motors. The nozzles of figure 5(a) are called original nozzles in this paper and are scaled versions of the type of nozzle used in the first stage of large ballistic missiles. These nozzles, which were used for jet-off tests only, are bell shaped with an equivalent divergence half-angle of 15° and an exit-to-throat area ratio of 8:1. The second set of nozzles (fig. 5(b)), herein called altered nozzles, were used in the hot-jet phase of the investigation. These altered nozzles have large center-body plugs which extend one-quarter of the jet-exit diameter beyond the nozzle exit and were designed to provide an annular jet with an external shape similar to that of the original nozzle at equal static-pressure ratios. (The external jet shape was derived from ref. 5.) The decomposition chamber was enlarged as compared with that of the original scaled version and the throat was removed, thus compromising the external shape to some extent. The plugs were secured to the nozzle by means of three vanes located symmetrically about the nozzle axis. Dimensional sketches of both the original and altered nozzles are given in figure 6, and a discussion of the jet-simulation problem is included in the appendix.

The rocket simulators were mounted in gimbal rings, allowing deflection of the nozzles in any direction. Each nozzle was restrained at preset angles of deflection in the pitch and lateral planes by a two-component strain-gage balance which measured moments about the gimbal axis. (See fig. 5(a).) The entire motor cage could be rotated 90°, thus allowing the nozzles to be either in a lateral or a vertical plane.

Turbopump-exhaust system.- In order to determine some of the effects of turbopump exhaust, two cylindrical nozzles were located in the base of the missile as indicated in figures 1 and 2. A total weight-flow rate of about 0.24 pound per second was obtained from nitrogen bottles for the jet-off tests and from a high-pressure air source for the jet-on tests.

Flow-survey apparatus.- A total-pressure survey rake (shown in the photograph in fig. 7 and in the dimensional sketch in fig. 8(a)) was used to obtain pressure profiles both at the model base and at the approximate exit plane of the nozzles. In both cases the nozzles were removed from the model.

Figure 8(b) shows a dimensional sketch of the ink-flow plate used to obtain flow patterns in a vertical plane at the base of the missile

(nozzles removed). A water-nigrosin (black dye) solution was emitted from 12 orifices shown in the plate in figure 8(b), and the resulting patterns on the white plate were photographed both with a still camera and with a motion-picture camera.

Instrumentation

Hinge moments in both the vertical and lateral planes were measured by means of two-component strain-gage balances located just ahead of the decomposition chambers. (See fig. 5(a).) For the jet-off tests, the output of the strain gages was fed through a digital converter and automatically punched into IBM cards for machine reduction to coefficient form. Jet-off skirt pressures and base pressures were recorded by photographing multitube mercury manometers.

In the jet-on tests, the electrical signals from the strain-gage balances and from electrical pressure transducers were transmitted to carrier amplifiers and then to recording oscillographs. The trace deflections on the recorder film were read manually and then converted to standard coefficients by machine computation.

The base temperatures were measured by three shielded chromel-alumel thermocouples and were recorded by a self-balancing potentiometer.

Tests

Jets off.- Hinge moments, base pressures, and skirt pressures were obtained through an angle-of-attack and angle-of-sideslip range from -9.5° to 5° at Mach numbers from 0.80 to 1.10 and at an average Reynolds number of 4×10^6 per foot. The original nozzles were tested at preset deflections from -8.7° to 0.2° in the pitch plane and from -2.8° to 6.2° in the lateral plane. For these tests the pitch plane was arbitrarily considered to be the plane containing the center lines of both nozzles at zero deflection. The nozzle deflections and hinge-moment coefficients presented in this paper are for the upper nozzle. Data for the lower nozzle are not presented because they are believed to be affected by the wake of the support strut, which, although very thin, altered the external-flow impingement on the lower nozzle in the pitch tests. For the yaw tests, the engine cage was rolled 90°, and the effect of strut wake on either nozzle was negligible. At all test conditions the deflections of the lower nozzle were the same as those of the upper nozzle in the lateral plane and were about 5.2° more positive in the pitch plane.

Jets on.- Because of the difficulty in obtaining jet-on hinge-moment data (due to simulation problems, propellant line restraints,

temperature effects, and so forth), it was desirable to obtain fairly extensive jet-off data to establish trends with angle of attack or nozzle deflection; a greatly reduced test program, then, would be sufficient to determine the jet effects. Accordingly, the jet-on data were obtained at the same Mach numbers as those for the jet-off tests but only at three angles of attack (0° and $\pm 5^\circ$) and primarily with one nozzle deflection (-5.7° in pitch plane and 0° in yaw plane); deflections in pitch of -3.1° and 0.3° were briefly investigated to establish jet-on trends with nozzle deflection.

Jet-on data were obtained with the altered nozzles (center-body plug) through a jet static-pressure-ratio range from about 1.5 to 2.4 for a nozzle deflection of 5.7°. For all other configurations, data were obtained only at a scheduled pressure ratio, that is, a pressure ratio corresponding to a given Mach number and altitude for a typical large missile. (See the appendix.) The static pressures were obtained from a static calibration of p_e plotted against weight flow; the pressure tubes were removed for the tunnel tests.

Tests at a Mach number of 1.10.- At a Mach number of 1.10, shock waves from the nose and the transition section combined and reflected from the top of the tunnel (nearest wall) onto or near the nozzles. This disturbance was sufficiently strong to increase base pressures and decrease hinge moments. In order to move this reflection downstream of the model, tests were made with a shortened second stage. Shadowgraphs indicated that the reflected wave was moved downstream about 1.5 model diameters. This change in model length had no effect on the hinge-moment data at subsonic speeds and a relatively small effect at a Mach number of 1.0. However, very large increases in hinge moment occurred at a Mach number of 1.10. Although a small part of this increase may be due to the actual change in model length (and a corresponding decrease in boundary-layer thickness), it is believed that most of the increase was due to the reduction in the interference effects of the reflected shock wave. In view of these results, all data in this paper for a Mach number of 1.10 were derived from the shortened model.

Flow studies.- Boundary-layer measurements at the base of the model were made through the Mach number and angle-of-attack range by means of a total-pressure survey rake. A wake-flow survey was also made by using the pressure rake at an axial station corresponding to the plane of the nozzle exits. In addition, visual flow studies were made at the base of the missile by using the ink-flow technique.

Accuracy and Corrections

The following tabulation presents the estimated accuracy of the coefficients and test parameters presented in this paper:

[redacted]

	Jets off	Jets on
$C_{h,V}$	±0.002	±0.015
$C_{h,L}$	±0.002	------
C_p	±0.005	±0.01
$p_{t,l}/p_{t,\infty}$	±0.01	
p_e/p_∞	------	±0.05
ΔT, ^oF		±2
α, β, θ, δ, deg	±0.1	±0.1
M	±0.005	±0.005

Because of asymmetry of the exhaust flow from the altered nozzles, the thrust vector did not coincide with the nozzle axis and thus produced hinge moments about the gimbal point. The nozzle hinge moments were, therefore, corrected for these tare loads, which were determined by static tests (wind tunnel off and jets on). The corrections were applied on the basis that the tare load variation with thrust was the same for the tunnel-on tests and the static tests.

A comparison of jet-off hinge-moment coefficients for the altered nozzle and the original nozzle indicated that the average difference was within the accuracy of the data for the angle-of-attack and Mach number range of these tests.

RESULTS

Jets Off

Typical total-pressure profiles in the boundary layer at the base of the model and in the wake at the nozzle-exit plane are presented in figure 9; lines of constant total pressure are presented in figure 10. Ink-flow photographs presented in figure 11 illustrate the wake flow including the effects of slotting the skirt. Shadowgraphs illustrating the shock pattern for the model-strut support system are shown in figure 12. Variations of hinge-moment coefficients with angle of attack and angle of sideslip for several nozzle deflections are shown in figures 13 and 14, respectively. Figures 15 and 16 show, respectively, the effect of skirt length and the effect of a slotted skirt on the vertical hinge-moment coefficient. Average base pressure coefficients for the basic-skirt and for the slotted-skirt configurations are presented in figure 17.

Jets On

The variations of vertical hinge-moment coefficient with static-pressure ratio and with nozzle deflection are shown in figures 18 and 19, respectively, and the effect of slotting the skirt is shown in figure 20. The variation of average base pressure coefficient with static-pressure ratio is presented in figure 21, and the effect of the slotted skirt is shown in figure 22. A comparison of the pressure distributions on the basic and slotted skirts is given in figure 23. Figure 24 shows the effects on base temperatures of slotting the skirt. Finally, shadowgraphs illustrating the effect of the jet exhaust on the shock pattern at the model base are presented in figure 25.

DISCUSSION

Flow Survey

Boundary-layer thickness.- Based on a one-seventh power-velocity distribution, the thickness of a turbulent boundary layer at the model base for the average test Reynolds number of 4×10^6 per foot is approximately 1 inch. Total-pressure profiles in the plane of the model base ($\phi = 0^\circ$), shown in figure 9, indicate a boundary-layer thickness of about 1 inch at an angle of attack of -5°. With increase in angle of attack to 0° and 5°, the pitot pressures attain a progressively smaller fraction of the free-stream total pressure and the boundary layer appears to be thicker than $1\frac{1}{2}$ inches (outermost tube on the survey rake). The thick boundary layer may be due to the blunt nose and a local rapid thickening of the boundary layer, although a contributing factor could also be the wake from a vernier rocket (see fig. 2) which was in line with the pressure rake.

Wake-flow convergence.- An additional total-pressure survey was made at an axial distance of 5.46 inches downstream of the model base (nozzles removed) which corresponds approximately to the plane of the nozzle exits. (See fig. 9(b).) In figure 10, points of equal total-pressure ratio at the two axial stations are connected with straight lines in order to indicate flow convergence. Presence of the nozzles may alter the convergence somewhat but some qualitative information can be derived by superimposing on the figure a sketch of the nozzle. This provides an indication of the impingement of the external stream on the nozzle. Except for relatively small impingement areas, indicated in figure 10, approximate base pressures exist on the entire nozzle surface. The lowest values of pressure ratio shown in figure 10 correspond to base pressures. It appears, then, that nozzle hinge moments are dependent

upon external stream impingement and base pressures and are, therefore, affected to a great extent by boundary-layer conditions at the model base. Reference 6 provides information concerning the interrelationship between boundary layer and base pressure.

Recirculation.- Some typical ink-flow patterns on the vertical splitter plate (see fig. 8(b)) are shown in figure 11 to illustrate the flow circulation at the base of the model (nozzles removed). For the basic-skirt configuration (figs. 11(a) and 11(b)) the patterns indicate the following: converging streamwise flow near the edges of the plate, forward flow near the center of the plate, and a ring vortex-type flow between these regions (clockwise on the upper half and counterclockwise on the lower half). The areas of these circulatory flows change with angle of attack, being nearly symmetrical at 0°. The forward flow in the center area causes a recirculation problem, that is, the entrainment of hot fuel-rich exhaust gases from the rocket nozzles and turbopump exhaust nozzles into the flow moving forward into the missile base.

One method of alleviating the base-recirculation problem is by venting the base by means of longitudinal slots such as those shown in figure 2. The effect on the wake flow of this slotted-skirt configuration at two representative Mach numbers is shown in figure 11(c). The flow through the slots tends to disrupt the vortex flow pattern and to decrease the forward flow. A fairly extensive study of the effects of various slots and slots with scoops on base flow and on base pressures can be found in references 1 and 7, respectively.

Shock-wave patterns.- Shadowgraphs showing the general shock-wave patterns for the complete model are presented in figure 12, and they indicate that shock waves from the support strut did not impinge on the model so as to interfere with nozzle hinge-moment measurements. Also shown are two strong shock waves at a Mach number of 1.10; one followed the flow overexpansion around the nose, and the other occurred ahead of the transition section and vernier nozzles. A thickening of the boundary layer associated with these shock waves would probably cause a reduction in the nozzle hinge moments.

Jet-Off Hinge Moments

Basic-skirt configuration.- Figure 13(a) shows the large increase in vertical hinge moments on the upper nozzle incurred by increasing nozzle deflection in the pitch plane. The results are as would be expected, considering the emergence of the nozzle from the body wake into the external stream flow. Rather unexpected, though, were the large hinge moments (for the larger nozzle deflections) at the positive angles of attack where it would be thought that the upper nozzle would be more shielded by the body from free-stream impingement. Apparently, downwash

associated with lifting vortices from the body was sufficient to cause external stream impingement on the nozzle, and thereby cause hinge moments at positive angles of attack of magnitude equal to those at comparable negative angles. Reference 8 indicates that a body with a blunt nose has a greater normal force at angles of attack than a body with a streamlined nose; therefore, it may be concluded that the lifting vortices and the downwash are stronger and the effect on hinge moments would also be greater. In general, the minimum hinge moments occurred near zero angle of attack at the higher deflection angles.

Simulated exhaust flow from the turbopump exhaust nozzles (nitrogen at a flow rate of 0.24 pound per second) had only a small effect on nozzle hinge moments. Some typical results are shown in figure 13(a) at a Mach number of 0.90.

In the range of test variables (α, β, M, δ, and θ) of this investigation, the lateral hinge moments were negligible, (See figs. 13(b) and 14.) Also shown in figure 14 are the small vertical hinge-moment coefficients incurred for a nozzle deflected in the yaw plane with the model tested through an angle-of-sideslip range.

Effect of skirt length.- The effect on vertical hinge moments of changing skirt length (see fig. 2) is indicated in figure 15. The long skirt reduced the exposed nozzle length from 5.46 inches (basic skirt) to 1.91 inches, a reduction which was sufficient to shield the nozzle completely from external air impingement and, therefore, reduce hinge moments to a negligible value. On the other hand, a small decrease in skirt length (exposed nozzle length of 6.99 inches) more than doubled the hinge moments as compared with those for the basic-skirt configuration. It is apparent that the optimum skirt length from an overall weight standpoint would be a compromise between weight reduction achieved with a minimum skirt and weight reduction achieved with minimum nozzle actuating structure (determined by nozzle hinge moments). Of course, other factors, such as base recirculation, will have to be considered.

Effect of slotted skirt.- It was believed that, in addition to alleviating the aforementioned recirculation problem, a slotted skirt might also reduce hinge moments by increasing base pressures and reducing external stream impingement. However, as shown in figure 16, the slotted skirt (see figs. 2 and 4) generally caused an increase in jet-off hinge-moment coefficient at Mach numbers up to 1.03. Only at a Mach number of 1.10 does the slotted skirt provide a reduction in hinge moments. At all test Mach numbers the slots actually decreased the base pressures (fig. 17) which would tend to increase hinge moments. Apparently, the slots decreased the external stream impingement at M = 1.10 and, thus, counteracted the effect of the decreased base pressures.

Jet-On Hinge Moments

Basic-skirt configuration.- The basic skirt in figure 18 shows that with the jets exhausting at the lowest value of static-pressure ratio of these tests (about 1.5), the vertical hinge moments were greatly increased over the jet-off values shown in figure 13(a). With increasing pressure ratio, however, the hinge moments decreased rapidly at all test Mach numbers. An explanation of this trend could be as follows: At low exhaust flows, the base pressures decreased as compared with those with jets off (see fig. 21), and the external stream was entrained so as to cause an increase in the force of impingement on the nozzle. As the pressure ratio was increased, the base pressures generally decreased further or remained constant, and thus, tended to produce large hinge moments. Apparently, however, the expansion of the jet bulb with increasing pressure ratio interfered with the external stream so as to decrease impingement on the nozzle and, thus, cause a reduction in hinge moments. Shadowgraphs in figure 25 illustrate the shock wave associated with impingement on the nozzle, with jets off, and the additional shock wave caused by the interaction of the jet exhaust with the external stream.

The rapid variation of vertical hinge-moment coefficient with nozzle deflection is shown in figure 19. It is shown here, as well as in figure 18 through a static-pressure-ratio range, that the maximum positive hinge moments for the range of nozzle deflections occurred at an angle of attack of 5° (maximum α of the jet-on tests). The average rate of change of $C_{h,V}$ with θ is roughly the same for the three angles of attack.

Effect of slotted skirt.- The slotted skirt reduced jet-on hinge moments at all test Mach numbers, except at $M = 0.90$, with a maximum reduction obtained at $M = 1.10$. (See fig. 20.) The reason for the ineffectiveness of the slots at a Mach number of 0.90 is not understood.

As indicated in figure 22, the slots decreased base pressures subsonically (tending to increase $C_{h,V}$) but increased base pressures at a Mach number of 1.00 and higher, with the greatest increase occurring at $M = 1.10$. The differences in base pressures between the basic and slotted skirt were not greatly affected by angle-of-attack changes; nevertheless, the slots were generally less effective in reducing $C_{h,V}$ at the positive angle of attack. This indicates that the flow through the slots for $\alpha = 5^\circ$ was less effective in reducing external stream impingement which was probably augmented by downwash from lifting vortices. From the foregoing, it appears that slots reduced hinge moments primarily by reducing impingement on the nozzle, although additional benefits were derived, of course, when the base pressures were also increased.

An important fact emerges from a comparison of the effects of slots on the jet-off and jet-on hinge-moment coefficients (figs. 16 and 20, respectively); namely, the effect of a vented skirt on jet-on nozzle hinge moments cannot be inferred from jet-off data. Not only can the magnitude of the effect be in error by several hundred percent, as shown at M = 1.10, but the direction of the change can be of opposite signs, as shown at the lower Mach numbers. Further, the base pressures by themselves are not a sufficient indication of the changes in hinge moments.

Skirt Pressures

At a Mach number of 0.90 (fig. 23(a)) the decrease in pressure just ahead of a slot (slots begin at $l/D = -0.41$) at $\phi = 0^\circ$ illustrates the expansion of the flow through the slot. Behind the slot, the pressure attain about the same value as that for the basic skirt and average base pressures were decreased. At $\phi = 15^\circ$, which is midway between two slots, the pressures were little affected. At Mach numbers of 1.00 and 1.10 (figs. 23(b) and 23(c), respectively) the pressures near the base at $\phi = 0^\circ$ were increased by the slots, as were the base pressures previously noted in figure 22. Again, the differences in pressures near the base at $\phi = 15^\circ$ were generally small.

Base Temperatures

The increase in temperature (jet on minus jet off) of the air recirculating into the base of the model was measured at three locations, as indicated in the sketch in figure 24. With a jet temperature of about 1,360° F, the increase in the entrained air temperatures for the basic-skirt configuration ranged from 71° F to 144° F. As expected, the largest temperature increments occurred near the center of the base. The slots reduced the temperature of the entrained air by 50 to nearly 100 percent through the Mach number and angle-of-attack range. Larger slots, or a combination of scoops and slots, would be more effective in reducing base recirculation. However, at the higher Mach numbers the stagnation temperatures of the incoming air can be a major problem.

SUMMARY OF RESULTS

A transonic wind-tunnel investigation of the nozzle hinge moments on a model of a large ballistic missile having two gimbaled rocket motors indicates the following results:

1. Nozzle hinge moments are a function of the external flow impingement and the base pressures and are, thus, dependent to a large extent on the boundary-layer conditions at the model base.

[redacted]

2. Either decreasing skirt length of increasing nozzle deflection causes increased impingement and, therefore, increased hinge moments.

3. Either increasing or decreasing the angle of attack from 0° increases nozzle hinge moments.

4. Nozzle hinge moments are generally increased with the jets operating. The jet effects are large at the low static-pressure ratios but decrease rapidly with increasing pressure ratio.

5. Generally, large reductions in jet-on nozzle hinge moments can be achieved by venting the skirt with longitudinal slots. With the same slotted skirt, however, jet-off hinge moments can be increased, thus indicating that the effects of a vented skirt with jets operating cannot be inferred from jet-off data. L 4 2 3

6. Longitudinal slots in the skirt reduce recirculation of the jet exhaust into the base and thereby reduce base temperatures.

Langley Research Center,
National Aeronautics and Space Administration,
Langley Field, Va., May 29, 1959.

APPENDIX

SIMULATION OF JET EFFECTS BY MEANS OF AN ANNULAR EXHAUST FROM NOZZLES HAVING LARGE CENTER BODIES

In the simulation of jet effects of convergent-divergent rocket nozzles, a problem may exist in obtaining the desired propellant weight-flow rates which either are beyond the capacity of the available system or which would require feed lines so large that they interfere with the desired measurements. Such was the case in the present investigation where an attempt was made to duplicate the jet effects of a convergent-divergent nozzle typical of large ballistic missiles. The nozzle had an exit-to-throat area ratio of 8:1, a Mach number of the exhaust gas of 3.0, a ratio of specific heats of 1.15, and a divergence half-angle of 15°. To simulate the actual jet shape for this nozzle would have required a weight-flow rate of about 15 pounds of H_2O_2 per second which is more than double the capacity of the present H_2O_2 system in the Langley 16-foot transonic tunnel. Furthermore, the objective of the investigation was to measure nozzle hinge moments with strain-gage balances and, since the propellant feed lines complicate these measurements, it was necessary to minimize the size of the feed lines, thus further restricting the flow rates.

The important parameter in evaluating the jet effects on aerodynamic hinge moments appeared to be jet shape, particularly on the initial portion of the jet exhaust. For a fixed nozzle divergence angle, the jet shape depends primarily on static-pressure ratio, and variations due to differences in jet Mach number and ratio of specific heats are relatively small. (See ref. 5.) Furthermore, it was not necessary to simulate thrust and, therefore, the momentum or exhaust velocity was considered to be of secondary importance. It was reasoned, then, that the jet shape and the static-pressure ratio could be obtained at greatly reduced weight flows by means of a nozzle having a large center body which would provide a relatively thin annular exhaust. Accordingly, a series of static tests were made to determine the jet boundaries for a nozzle having center bodies of varying external lengths, exit areas, and divergence angles. The boundaries were determined both by shadowgraphs (see fig. 26) and by total-pressure measurements at two axial locations by means of a traversing probe. Chamber pressures, weight flows, and exit static pressures were also measured.

The jet boundaries for the nozzle with various center bodies were then compared with the theoretical boundaries for the full-flowing nozzle

as determined from reference 5. Some results for the flared plug (see fig. 6) selected for the wind-tunnel tests are shown in figure 27. This plug extended one-quarter of the nozzle-exit diameter beyond the exit plane and provided a 0.34-inch-thick annular exhaust at a Mach number of 1.0. The advantage in using a sonic exit is that it provides the thickest jet annulus for a given weight flow and static-pressure ratio. As indicated in figure 27, in order to obtain good boundary simulation, a static-pressure ratio somewhat higher than the assumed values used to calculate the theoretical jet shape of the full-flowing nozzle exhaust was required. A comparison of the static-pressure-ratio schedule for a typical ballistic missile flight with the pressure-ratio schedule used to obtain boundary simulation in the model tests is shown in figure 28.

REFERENCES

1. Collins, J. D.: Wind Tunnel Studies on Titan Stage I - Base Pressures, Aerodynamic Nozzle Hinge-Moments, and Engine Compartment Recirculation. WDD-M-SR-58-39 (Contract AF04(645)-56), The Martin Co., Aug. 1958.

2. Few, Albert G., Jr.: Experimental Results of Some Effects of the Interaction Between a Hot Propulsive Jet and Several Tailless Missile Afterbody Configurations Immersed in External Flow. Tech. Rep. No. DA-TR-6-58, Dev. Operations Div., Army Ballistic Missile Agency (Redstone Arsenal, Ala.), May 1958.

3. Ward, Vernon G., Whitcomb, Charles F., and Pearson, Merwin D.: Air-Flow and Power Characteristics of the Langley 16-Foot Transonic Wind Tunnel With Slotted Test Section. NACA RM L52E01, 1952.

4. Runckel, Jack F., and Swihart, John M.: A Hydrogen Peroxide Hot-Jet Simulator for Wind-Tunnel Tests of Turbojet-Exit Models. NASA MEMO 1-10-59L, 1959.

5. Love, Eugene S., Woodling, Mildred J., and Lee, Louise P.: Boundaries of Supersonic Axisymmetric Free Jets. NACA RM L56G18, 1956.

6. Kurzweg, H. H.: Interrelationship Between Boundary Layer and Base Pressure. Jour. Aero. Sci., vol. 18, no. 11, Nov. 1951, pp. 743-748.

7. Nelson, William J., and Scott, William R.: Jet Effects on the Base Drag of a Cylindrical Afterbody With Extended Nozzles. NACA RM L58A27, 1958.

8. Polhamus, Edward C.: Effect of Nose Shape on Subsonic Aerodynamic Characteristics of a Body of Revolution Having a Fineness Ratio of 10.94. NACA RM L57F25, 1957.

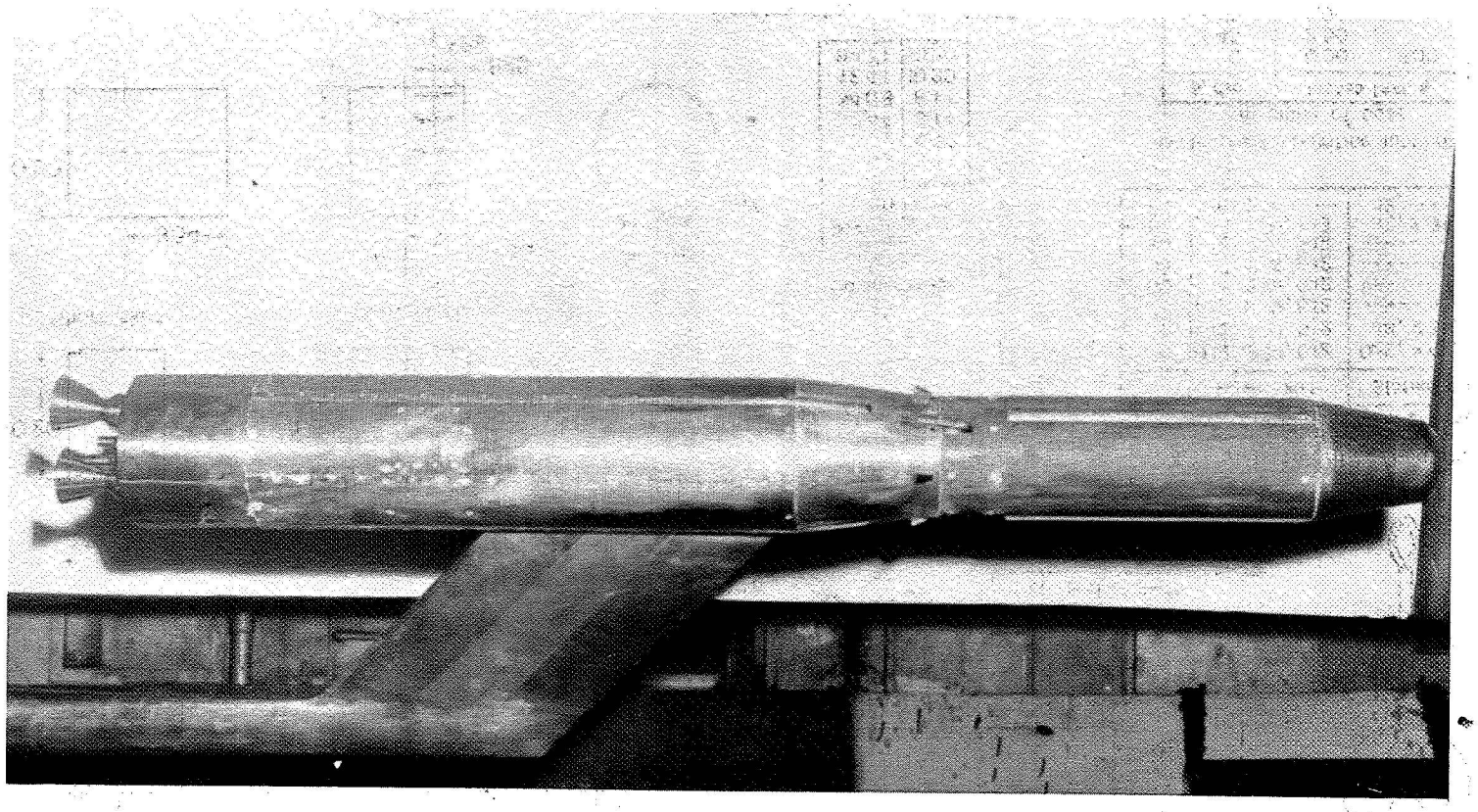

L-57-1264

Figure 1.- Photograph of basic model mounted in tunnel.

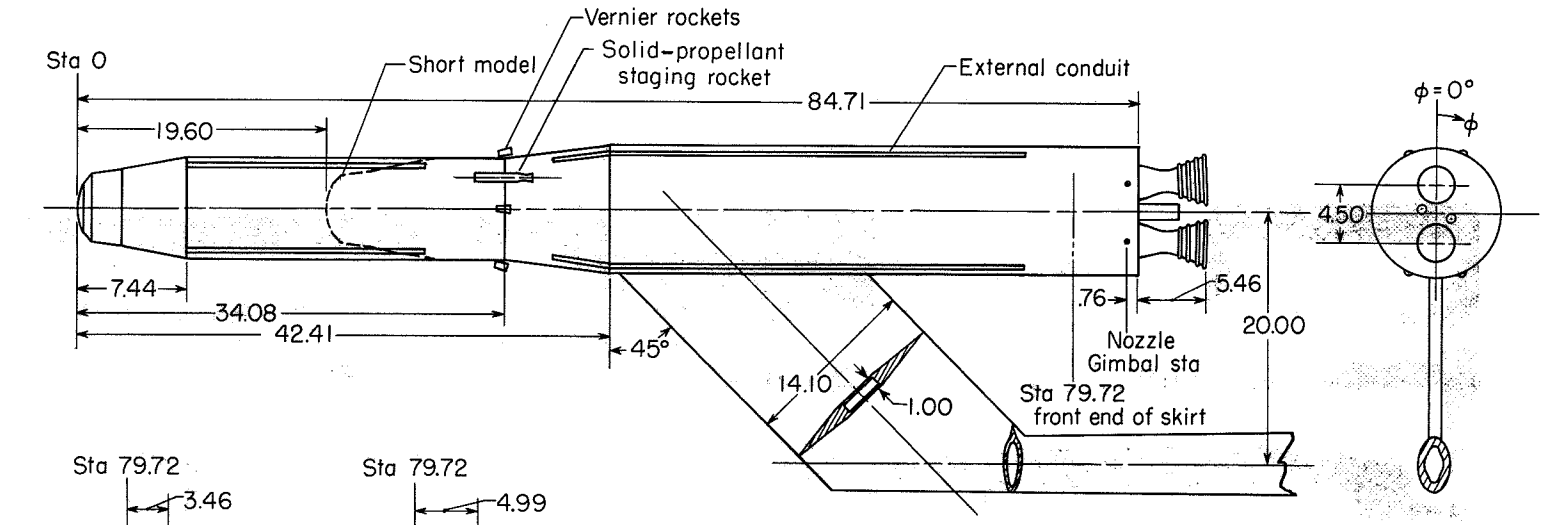

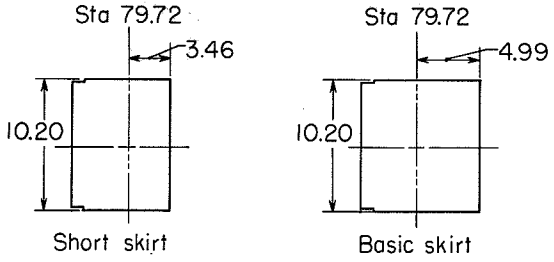

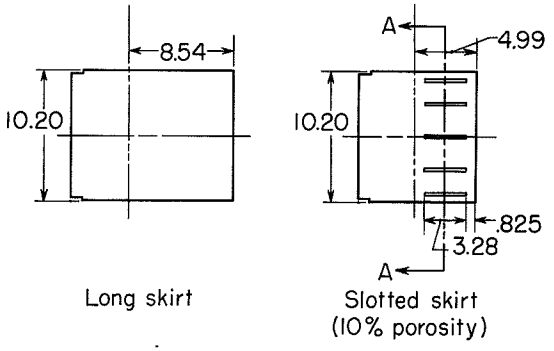

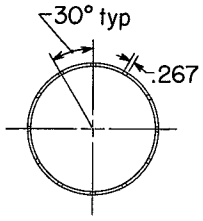

Basic model dimensions

Station	Dia.
0.00	0.00
.34	4.04
1.00	5.37
3.39	6.08
7.44	8.11
34.08	8.11
42.41	10.20
84.71	10.20

Fineness ratio,----------8.300
Frontal area,----------0.567 ft sq
Nozzle-exit diameter,-----3.666 in.

Skirt-pressure-orifice location

φ, deg	Inches upstream of base	
	Basic skirt	Slotted skirt
0	0.12, 2.31, 6.12	0.12, 4.41, 6.12
15	.12, 2.31, 6.12	.12, 2.31, 6.12
45	.12, 2.31, 6.12	----------
60	.12, 2.31, 6.12	----------
75	.12, 2.31, 6.12	----------
90	.12, 2.31, 6.12	----------
165	.12, 2.31, 6.12	.12, 2.31, 6.12
180	.12, 2.31 ----	.12,-----6.12

Base-pressure-orifice locations in plane of base

φ, deg	Inches from ℄	
0	0.00	5.00
±45	2.50	
±90	5.00	
±135	2.35	
180	5.00	

Figure 2.- Dimensional sketch of model. All linear dimensions are in inches.

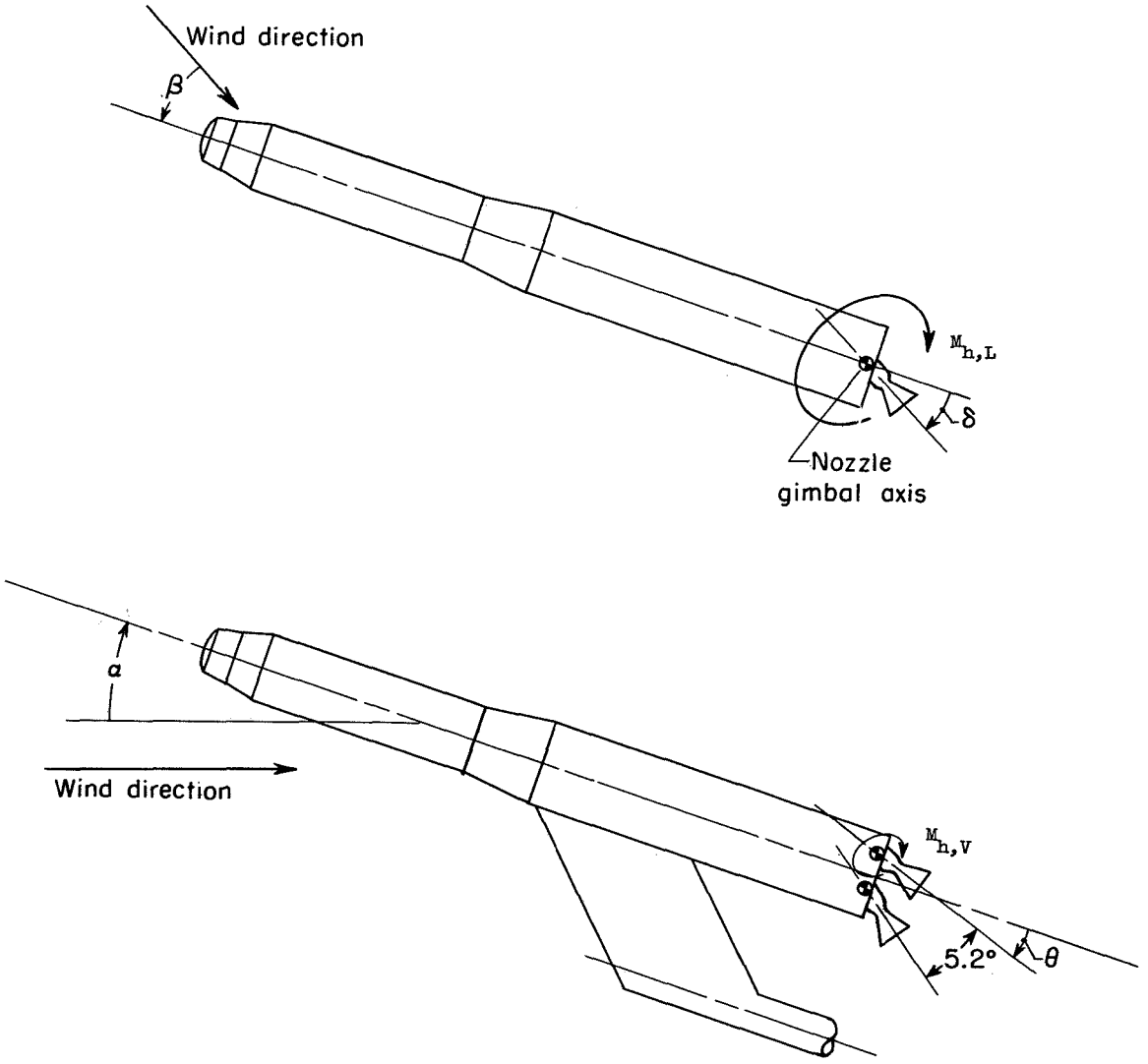

Figure 3.- Sign convention for model. Arrows indicate positive direction of moments and angles.

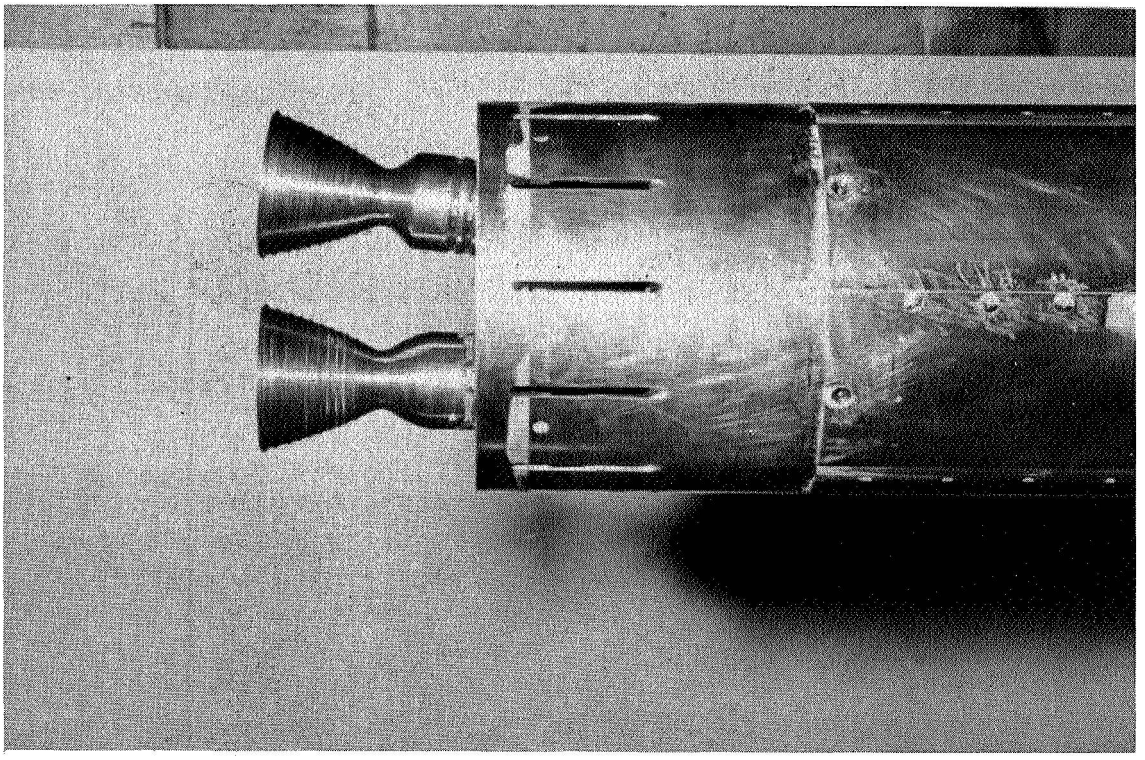

L-58-1465

Figure 4.- Photograph of slotted skirt. $\theta = -5.7^{\circ}$.

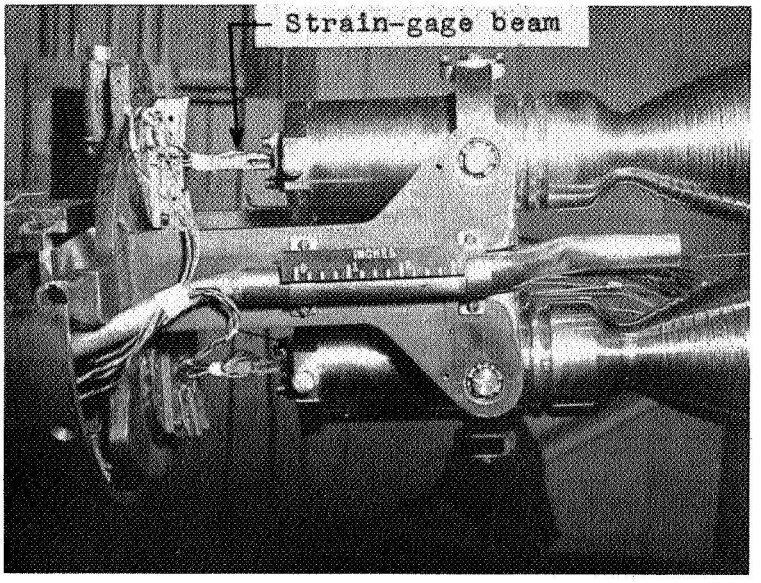

(a) Original scaled nozzles and hinge-moment beams; afterbody shell removed.

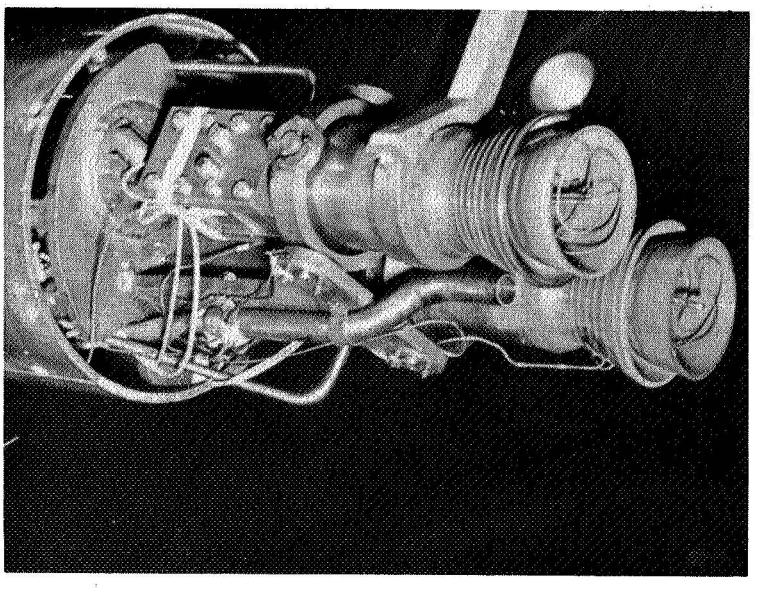

L-59-3036

(b) Altered nozzles; calibration fixture for moment gages attached to one nozzle.

Figure 5.- Photographs of original and altered rocket-motor nozzles.

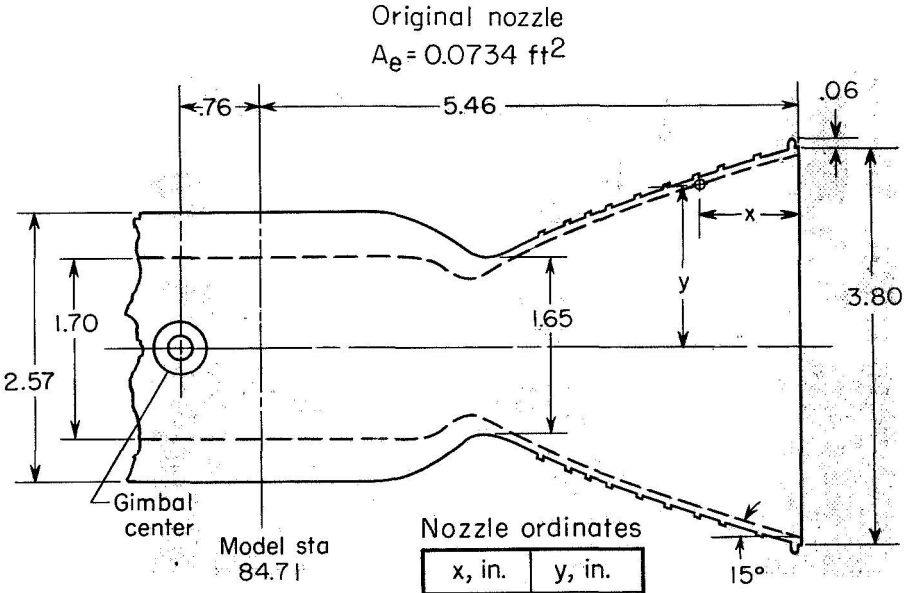

Nozzle ordinates

x, in.	y, in.
0	1.833
1.701	1.283
2.551	.911
3.103	.648
3.751	.847

Nozzle ordinates

x, in.	y, in.	R, in.
0.42	1.73	1.23
.85	1.60	1.10
1.28	1.45	.85
1.70	1.28	.40

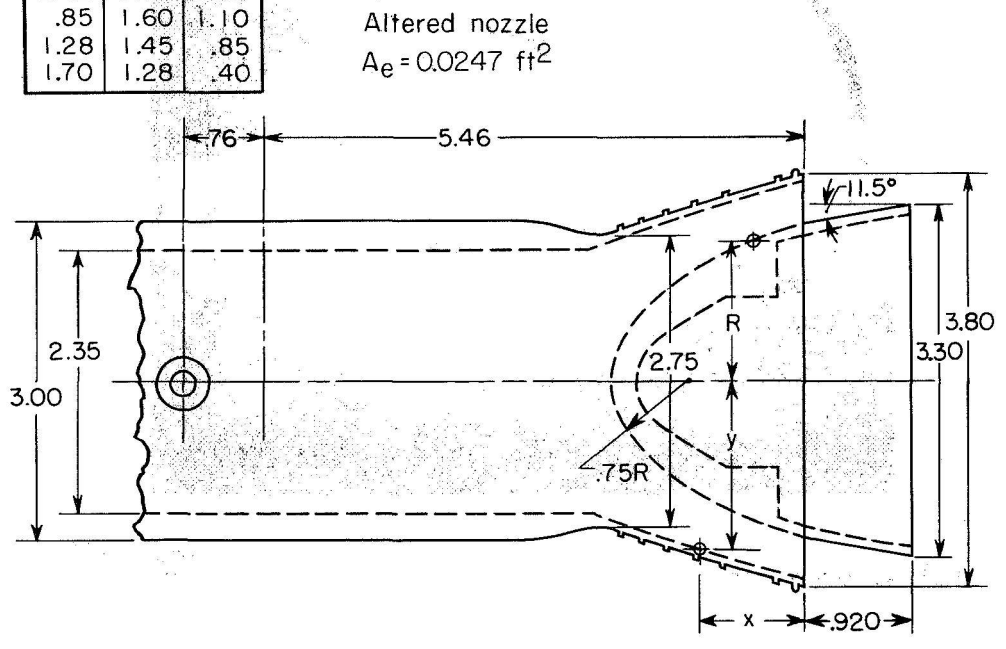

Figure 6.- Dimensional sketches of original and altered nozzles.

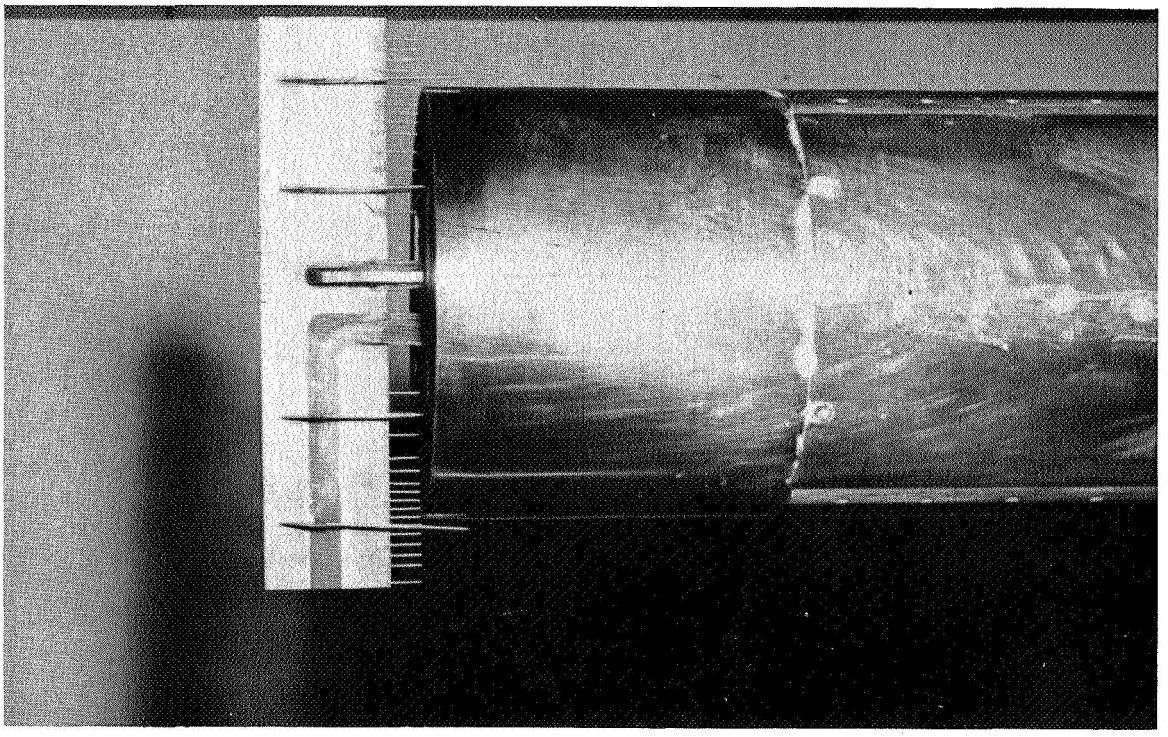

L-423

L-58-1365

Figure 7.- Photograph of boundary-layer rake at base of missile.

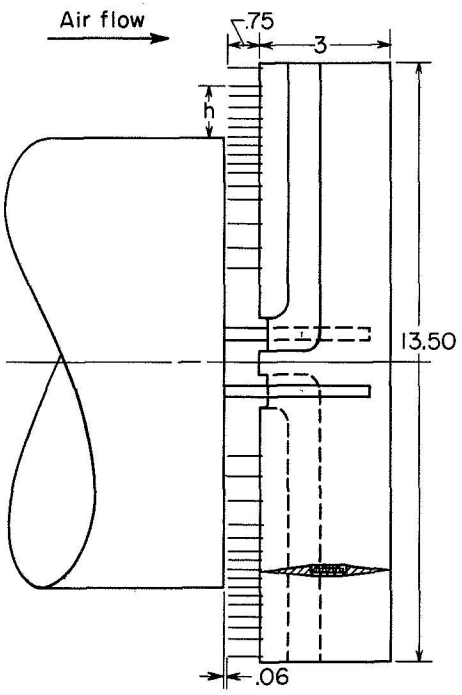

Probe location

No.	h
1	1.55
2	1.15
3	.90
4	.65
5	.40
6	.20
7	.00
8	-.20
9	-.40
10	-.60
11	-.80
12	-1.10
13	-1.50
14	-1.95
15	-2.45
16	-2.95

(a) Total pressure rake

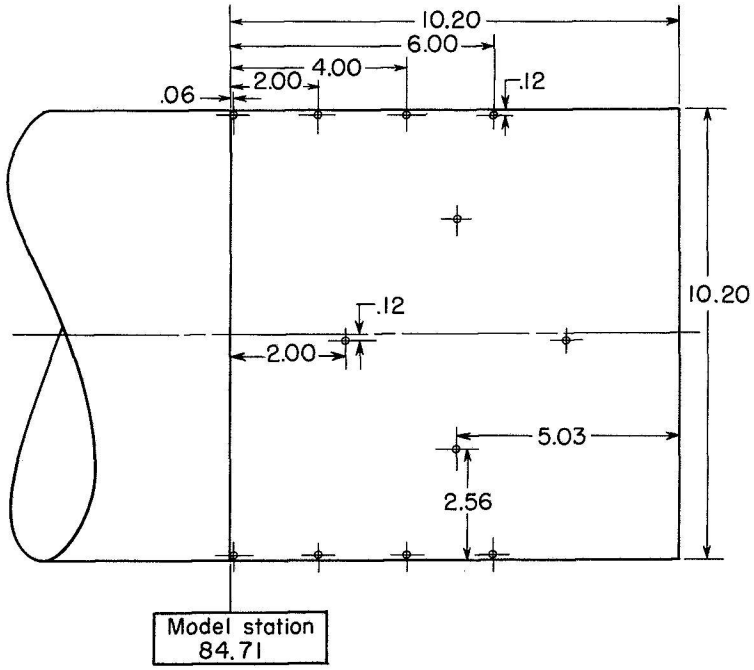

(b) Ink-flow plate, orifice locations

Figure 8.- Dimensional sketch of flow survey apparatus. All dimensions are in inches.

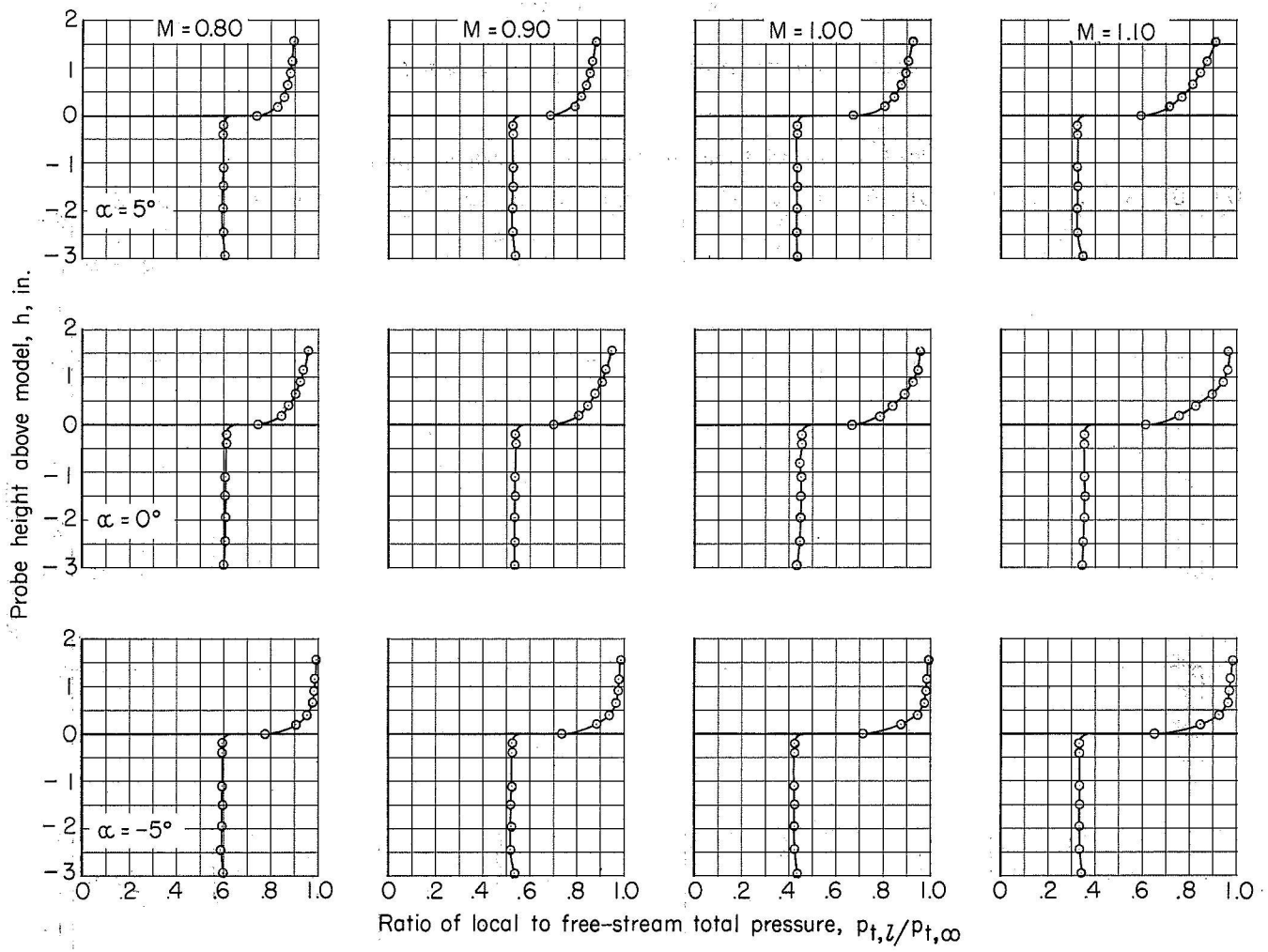

(a) Rake 0.06 inch rearward of model.

Figure 9.- Total-pressure survey at base of model. Basic skirt; nozzles removed; $\phi = 0^{\circ}$.

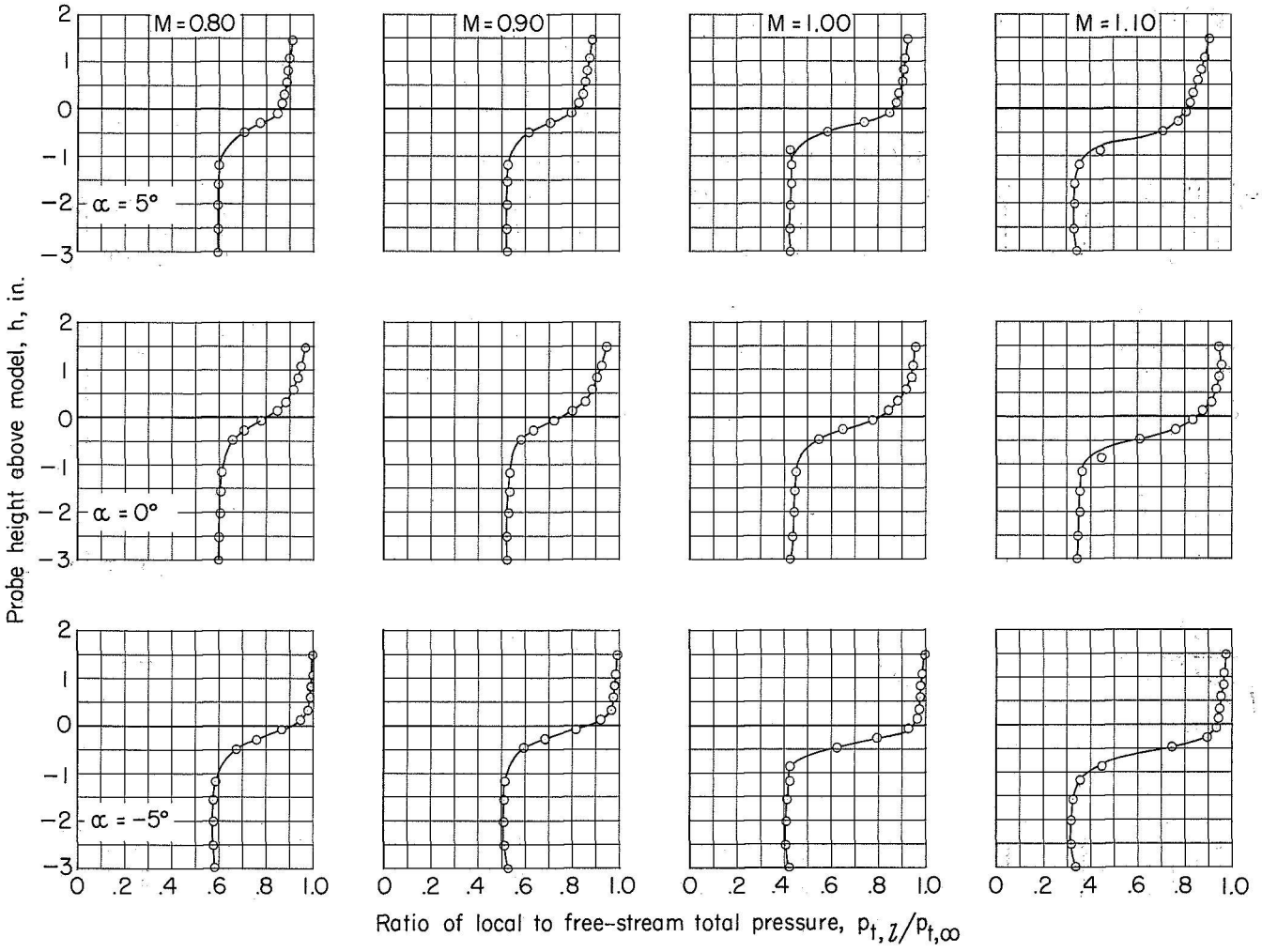

(b) Rake 5.46 inches rearward of model.

Figure 9.- Concluded.

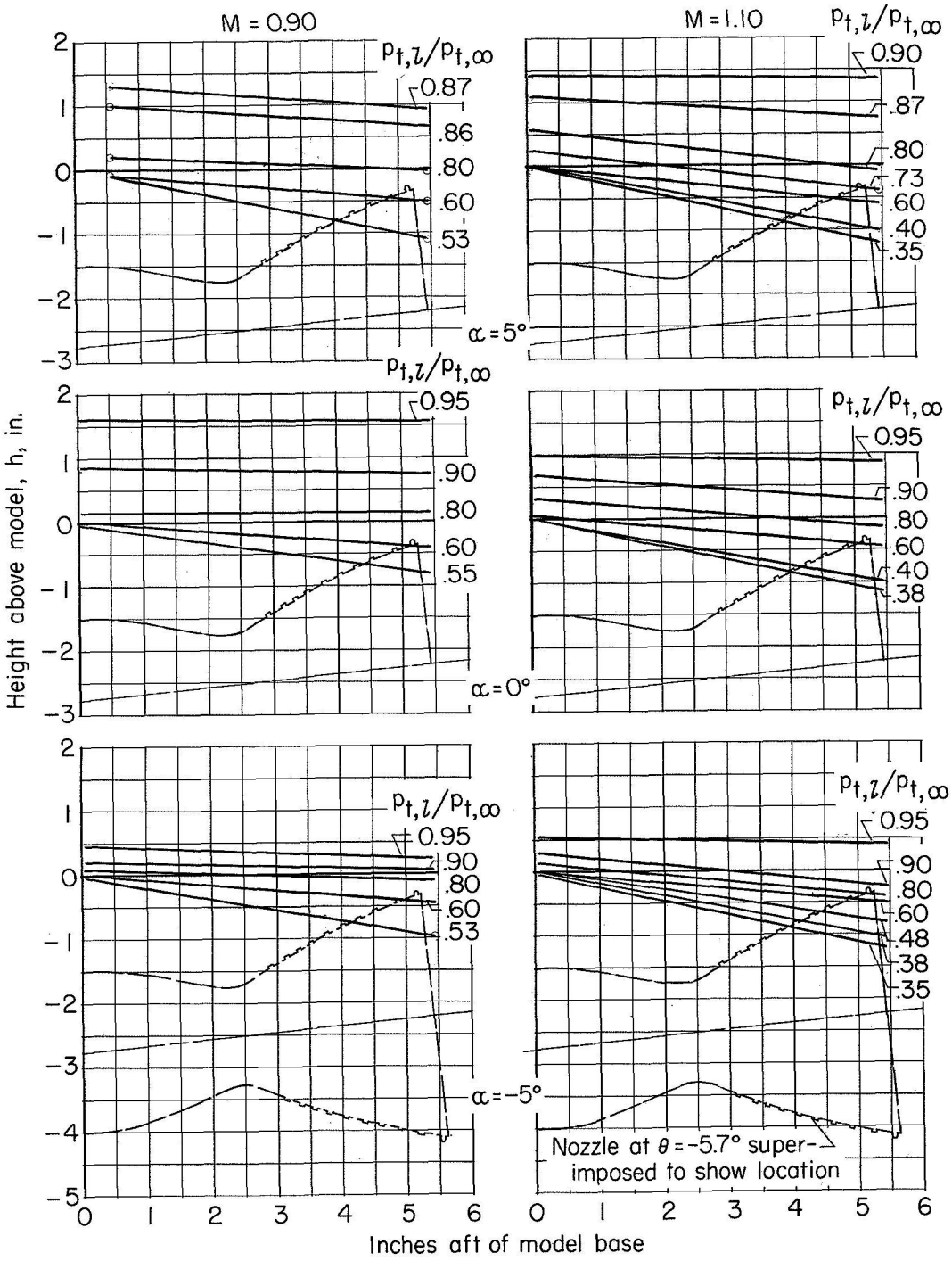

Figure 10.- Convergence of wake flow at base of model. Basic skirt; nozzles removed.

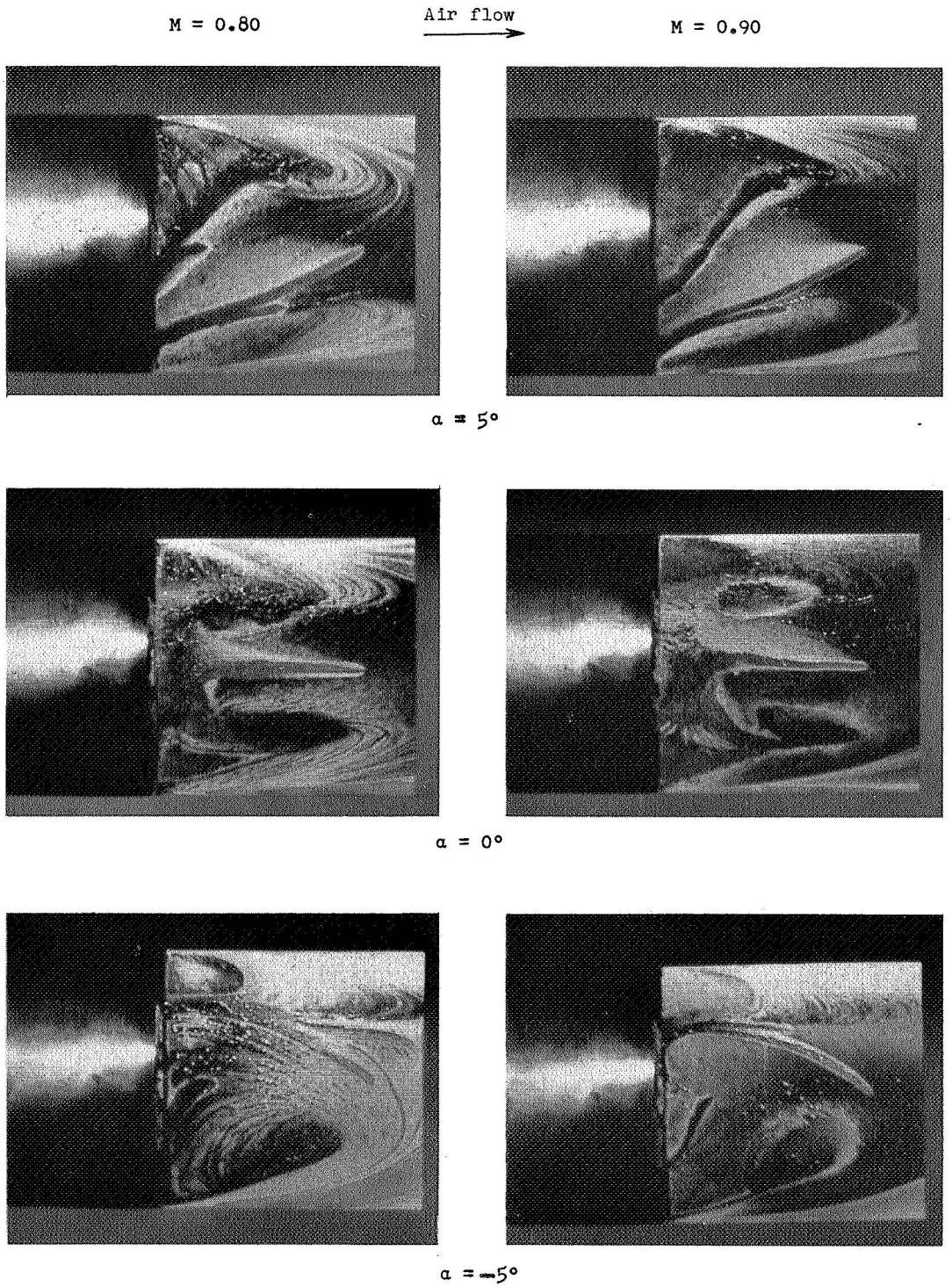

L-423

(a) Basic skirt; M = 0.80 and 0.90. L-59-3037

Figure 11.- Ink-flow photographs illustrating wake flow at base of model. Basic and slotted skirts; nozzles removed.

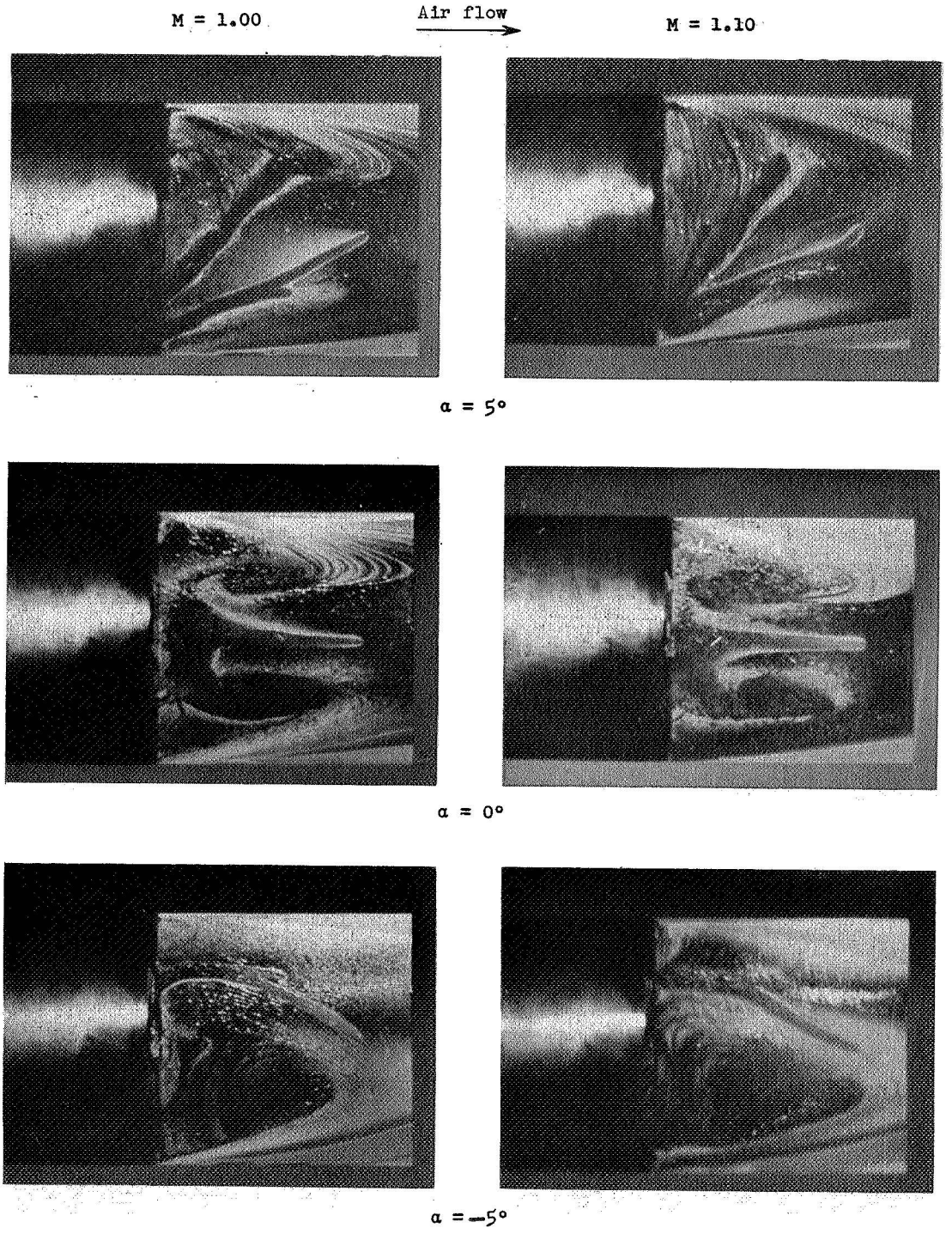

L-423

(b) Basic skirt; M = 1.00 and 1.10. L-59-3038

Figure 11.- Continued.

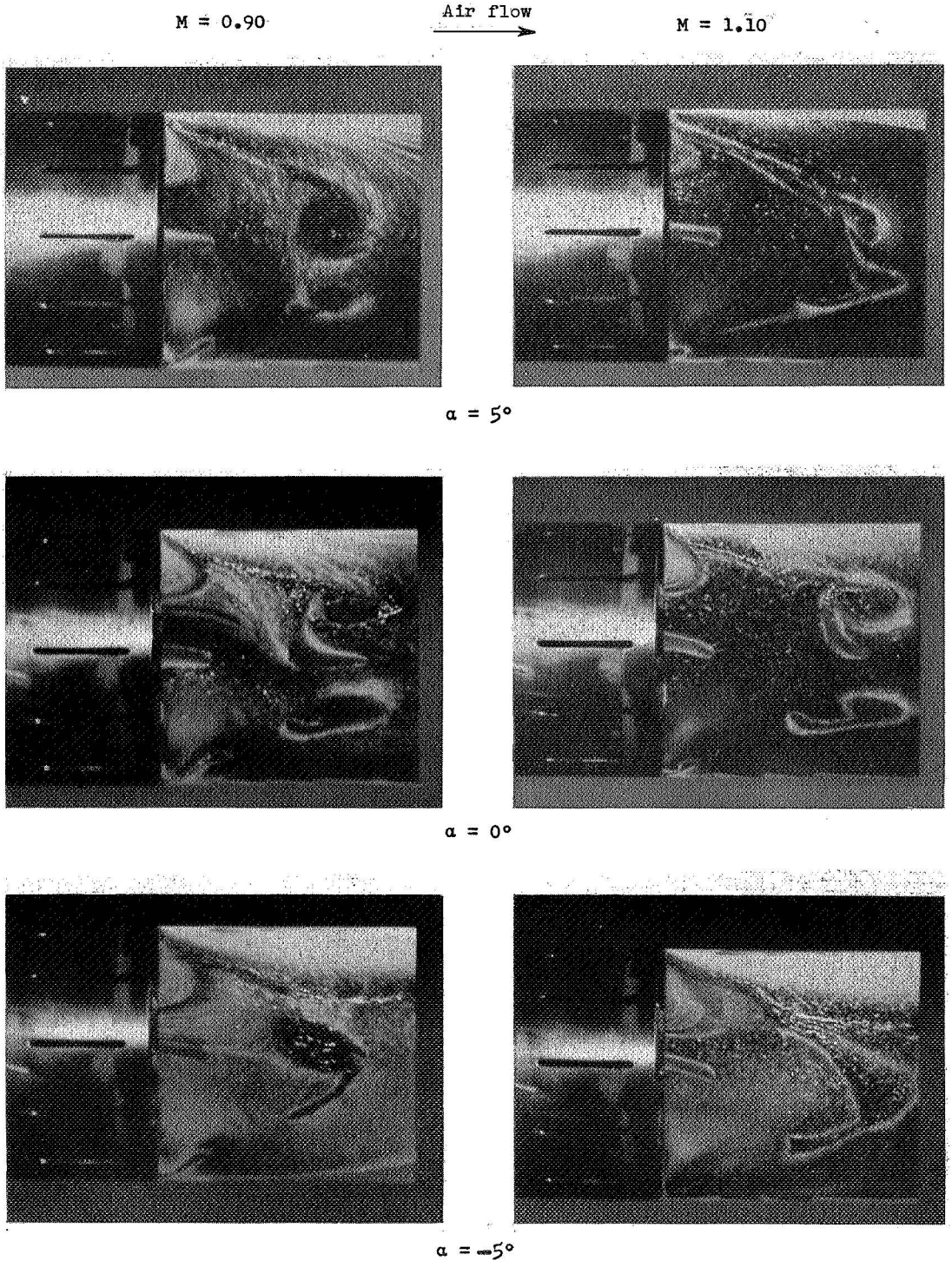

L-423

(c) Slotted skirt; M = 0.90 and 1.10. L-59-3039

Figure 11.- Concluded.

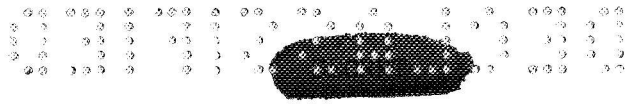

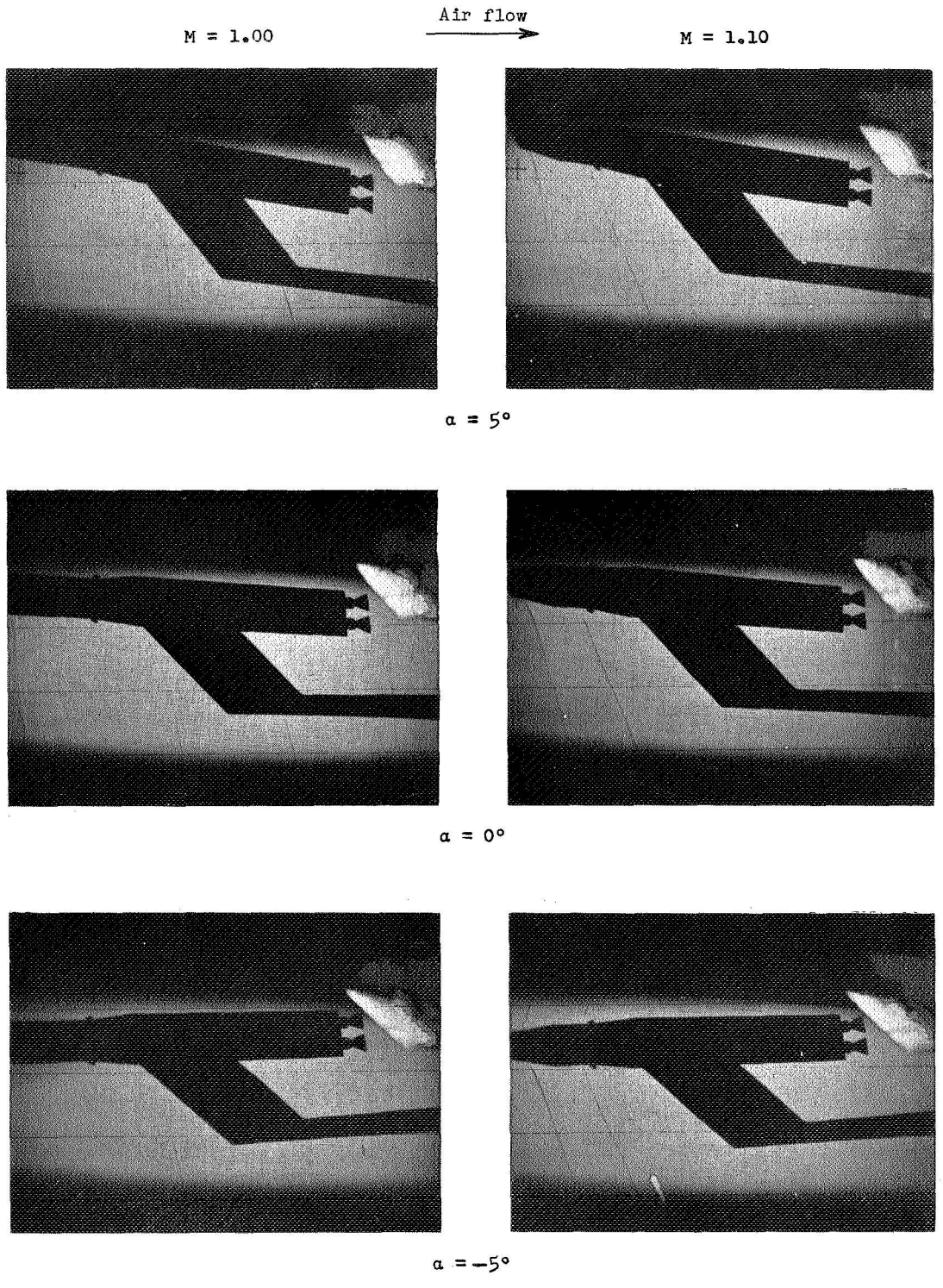

Figure 12.- Shadowgraphs of model. Jets off. L-59-3040

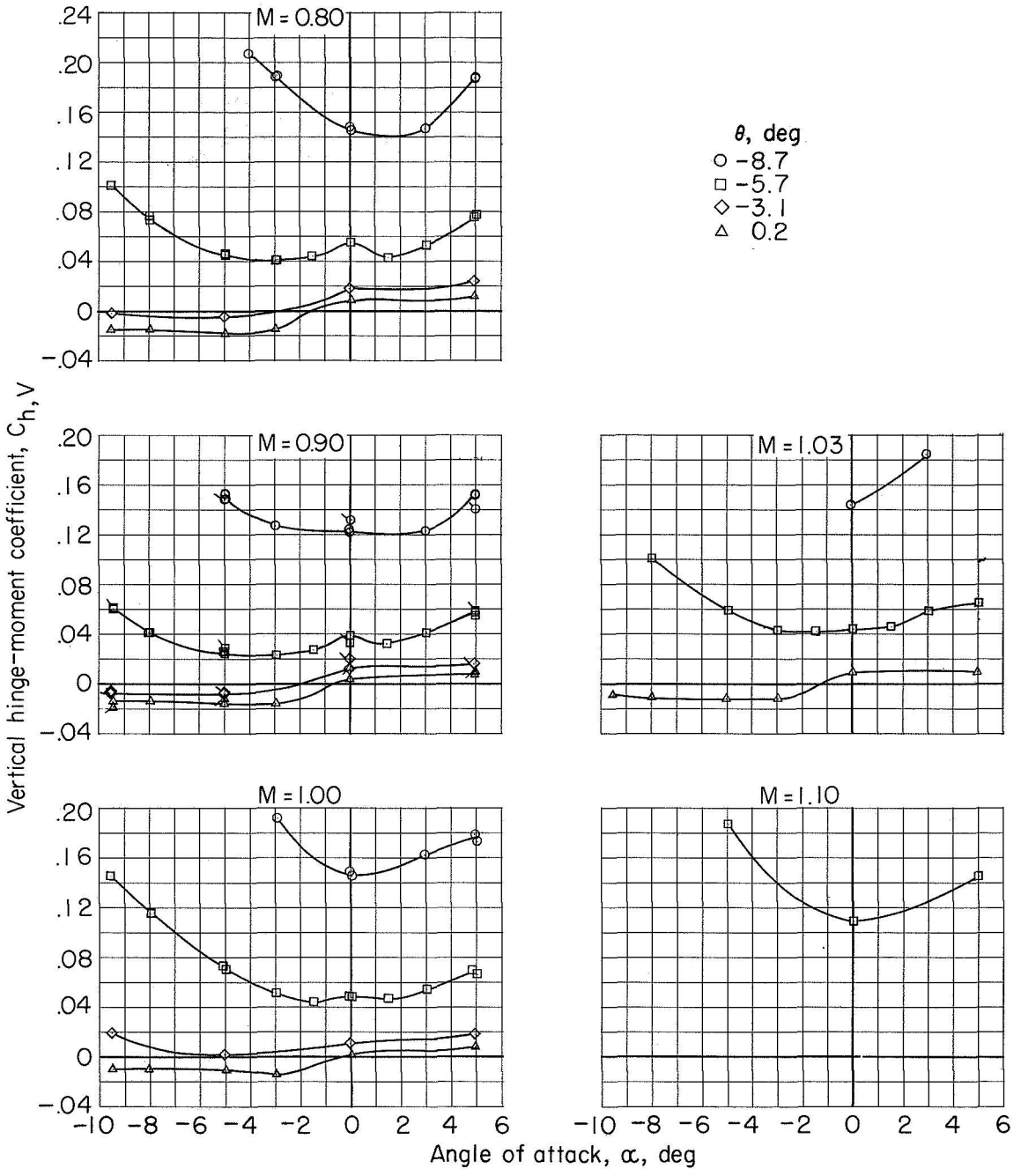

(a) Vertical hinge-moment coefficient $C_{h,V}$.

Figure 13.- Variation of hinge-moment coefficient with angle of attack for several nozzle deflections in the pitch plane. Upper nozzles; basic skirt; jets off; $\delta = 0^{o}$. Flagged symbols indicate turbopump on.

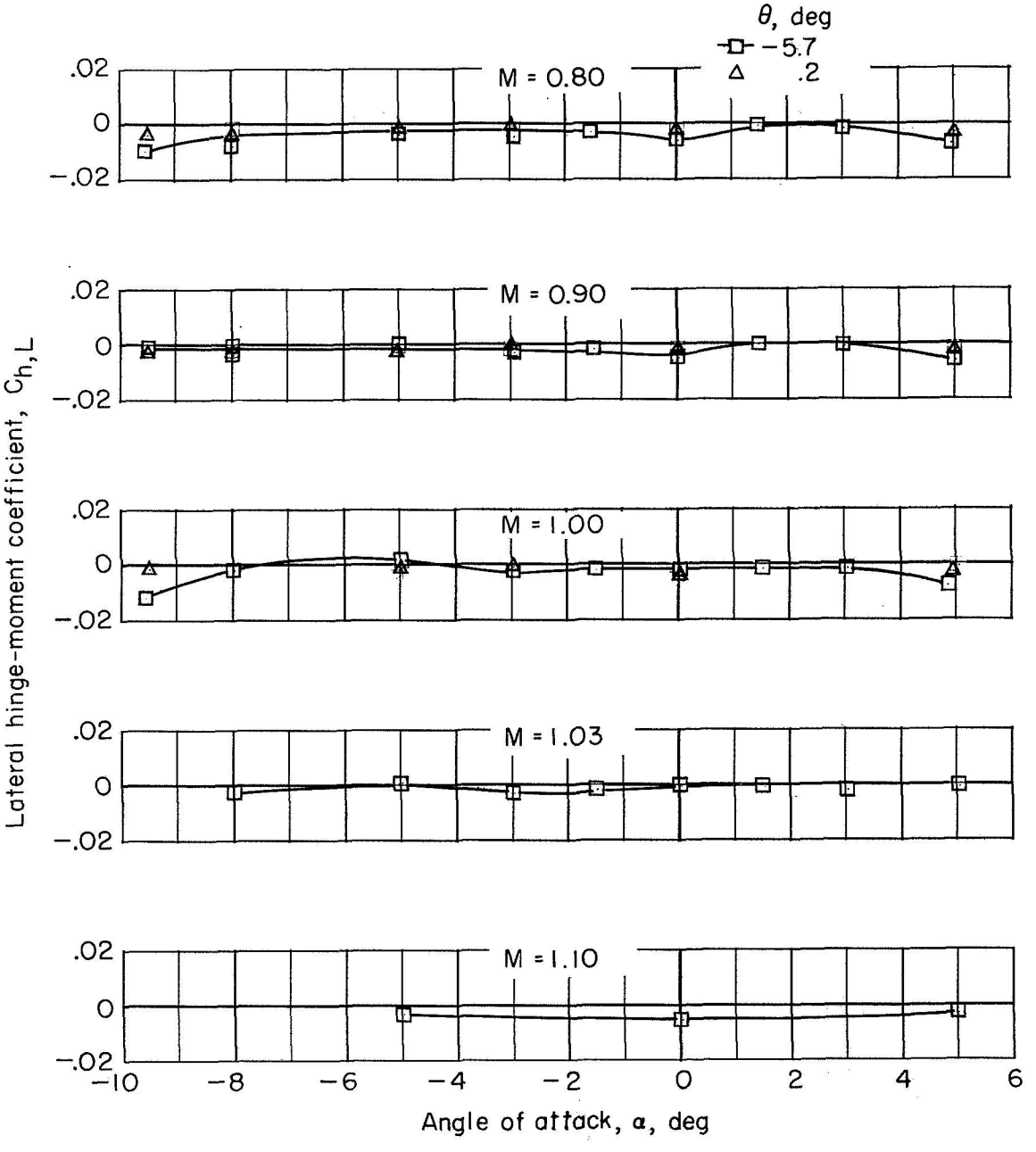

(b) Lateral hinge-moment coefficient $C_{h,L}$.

Figure 13.- Concluded.

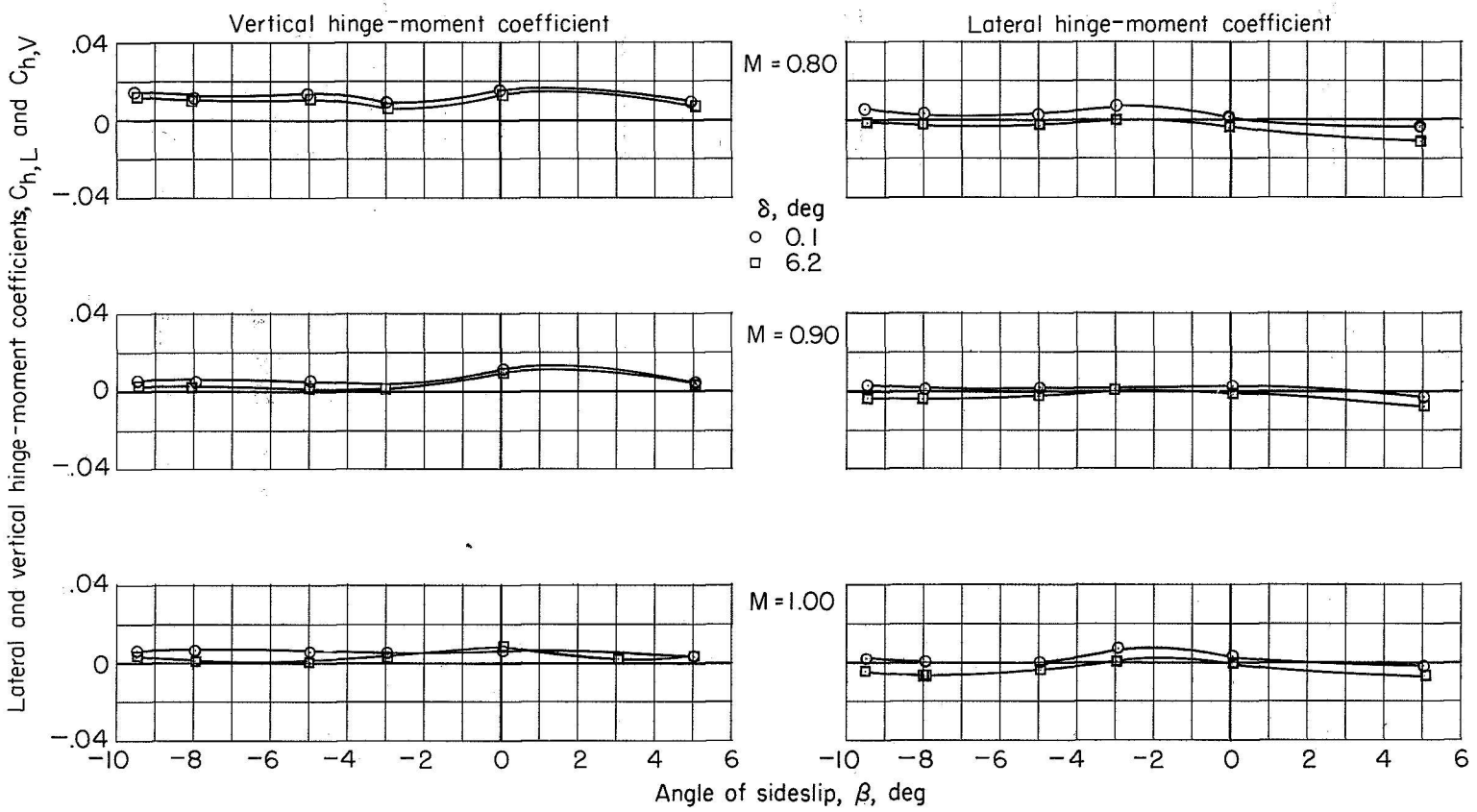

Figure 14.- Variation of hinge-moment coefficient with angle of sideslip for two nozzle deflections in the lateral plane. Upper nozzles; jets off; $\alpha = 0^{\circ}$; $\theta = 0^{\circ}$.

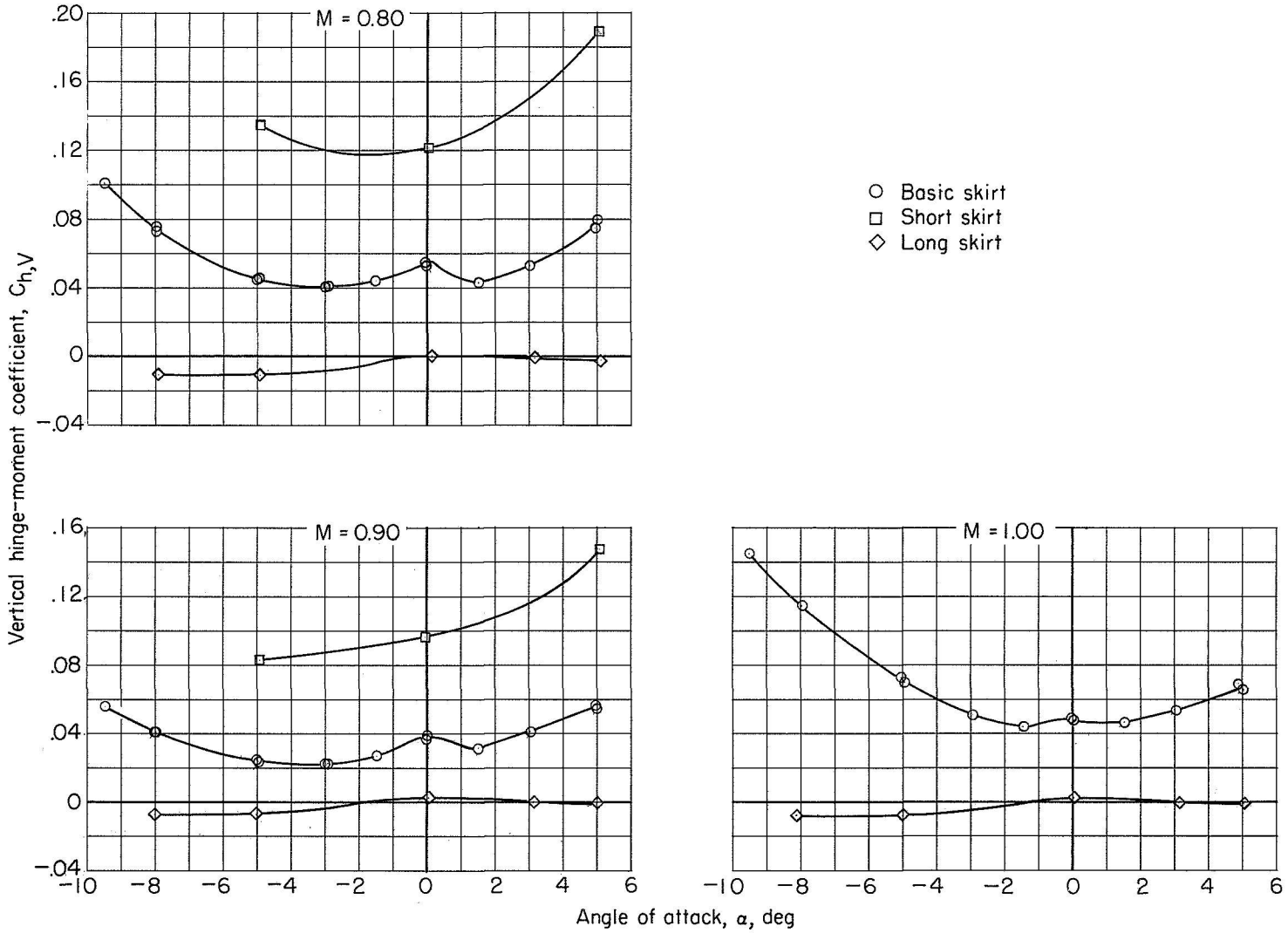

Figure 15.- Effect of skirt length on vertical hinge-moment coefficient. Upper nozzles; jets off; $\theta = -5.7^{\circ}$; $\delta = 0^{\circ}$.

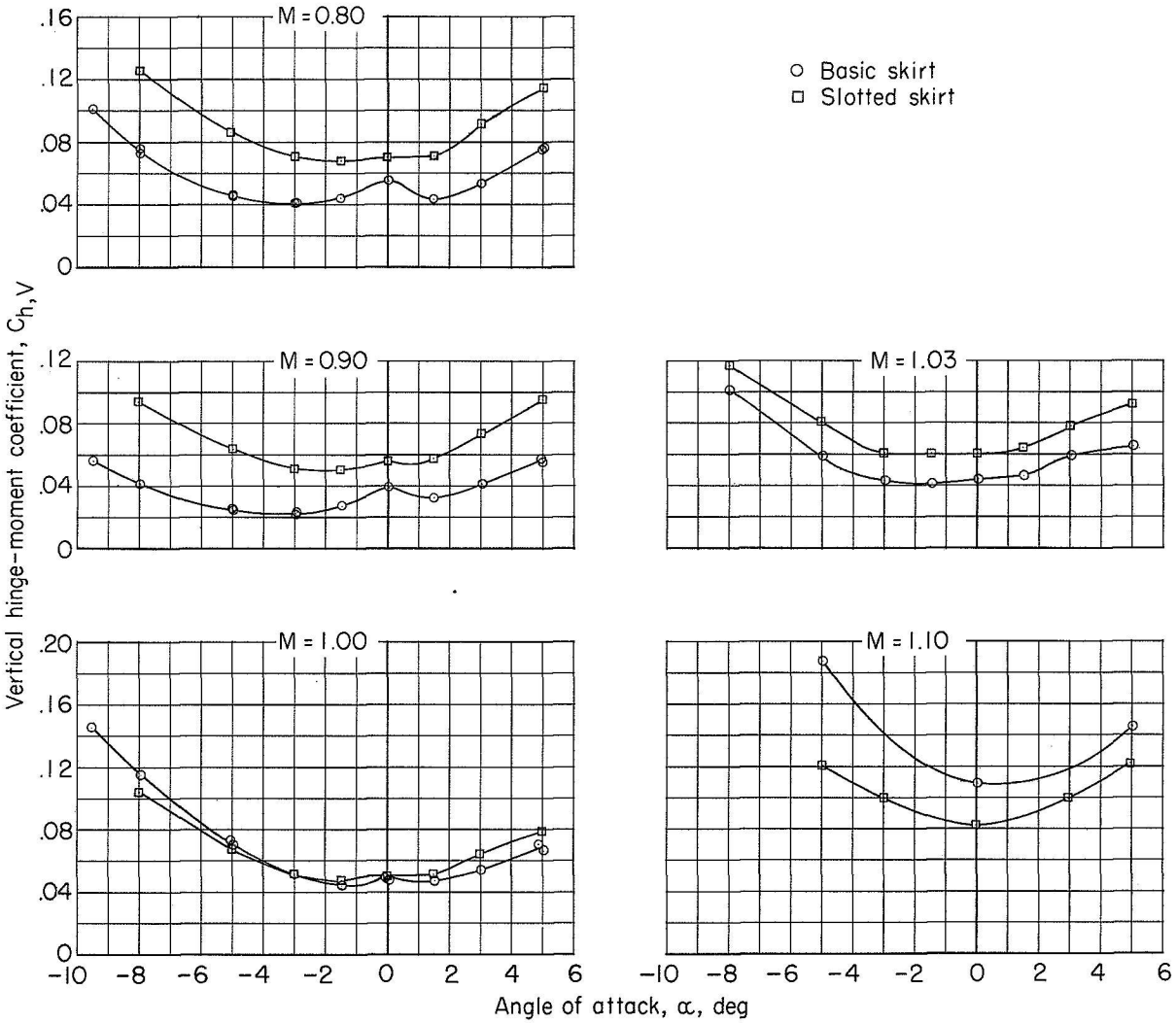

Figure 16.- Effect of slotted skirt on vertical hinge-moment coefficient. Upper nozzles; jets off; $\theta = -5.7^{\circ}$; $\delta = 0^{\circ}$.

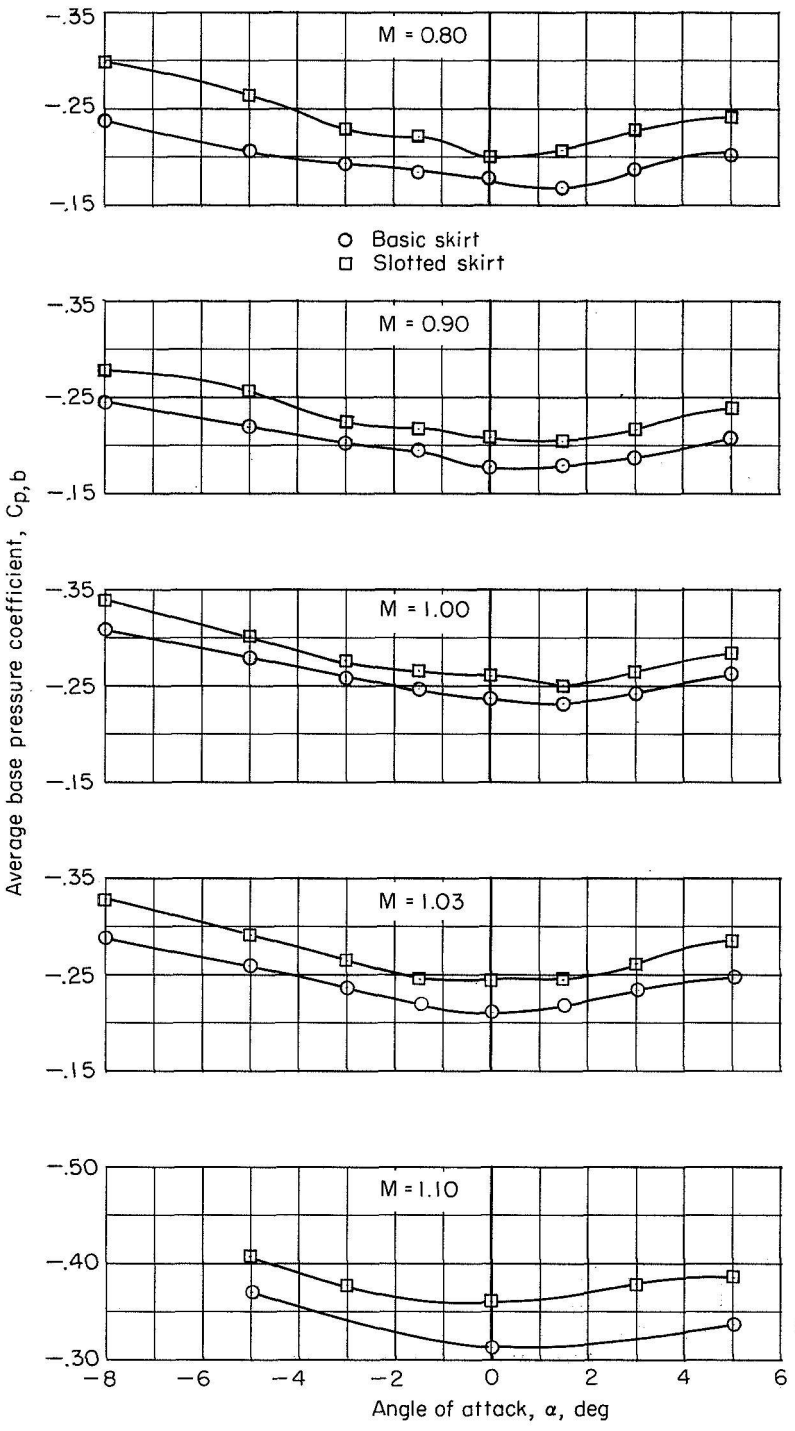

Figure 17.- Effect of slotted skirt on average base pressure coefficient. Original nozzles; jets off; $\theta = -5.7^{\circ}$; $\delta = 0^{\circ}$.

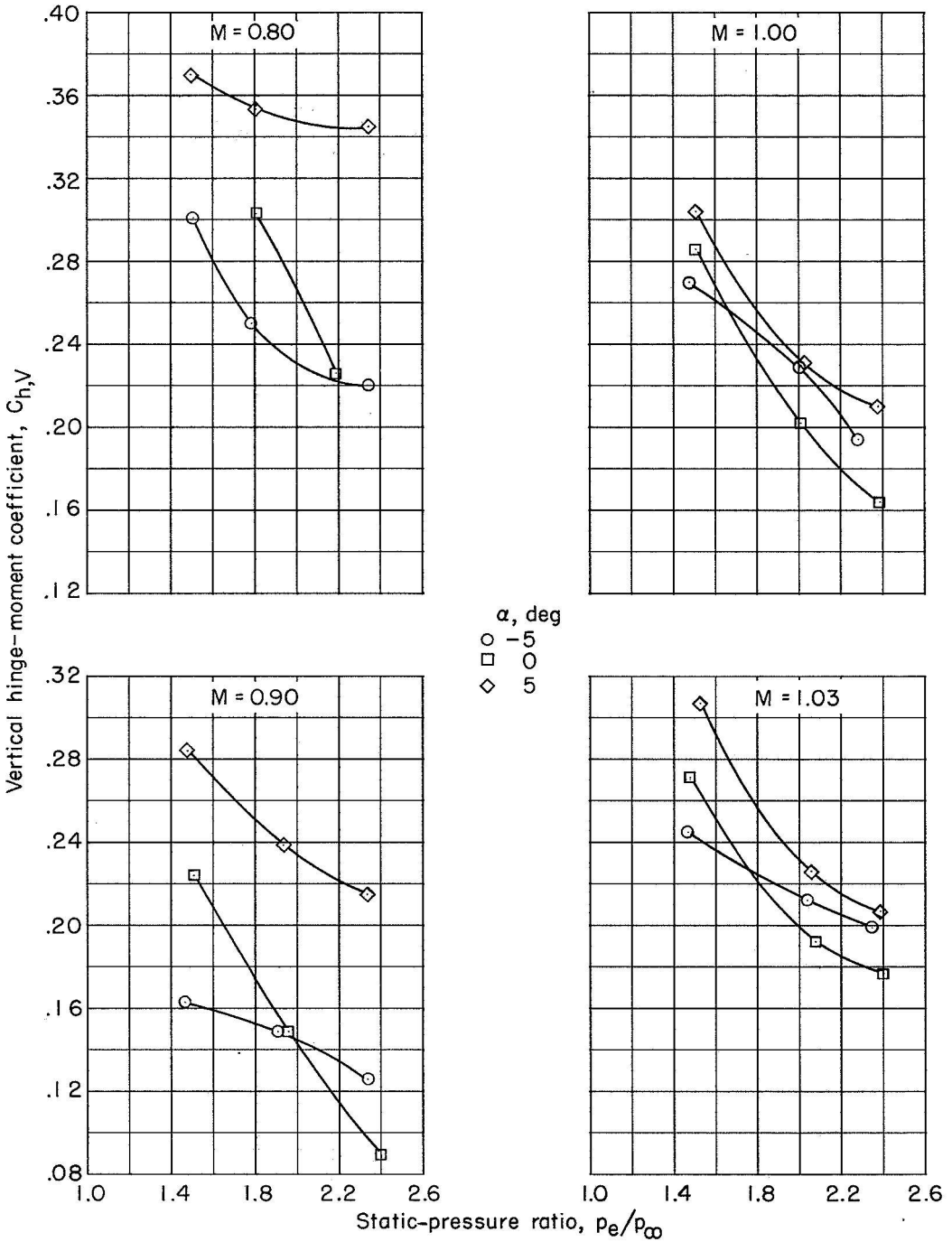

Figure 18.- Variation of vertical hinge-moment coefficient with static-pressure ratio of upper nozzle. Altered nozzles; basic skirt; $\theta = -5.7^\circ$; $\delta = 0^\circ$.

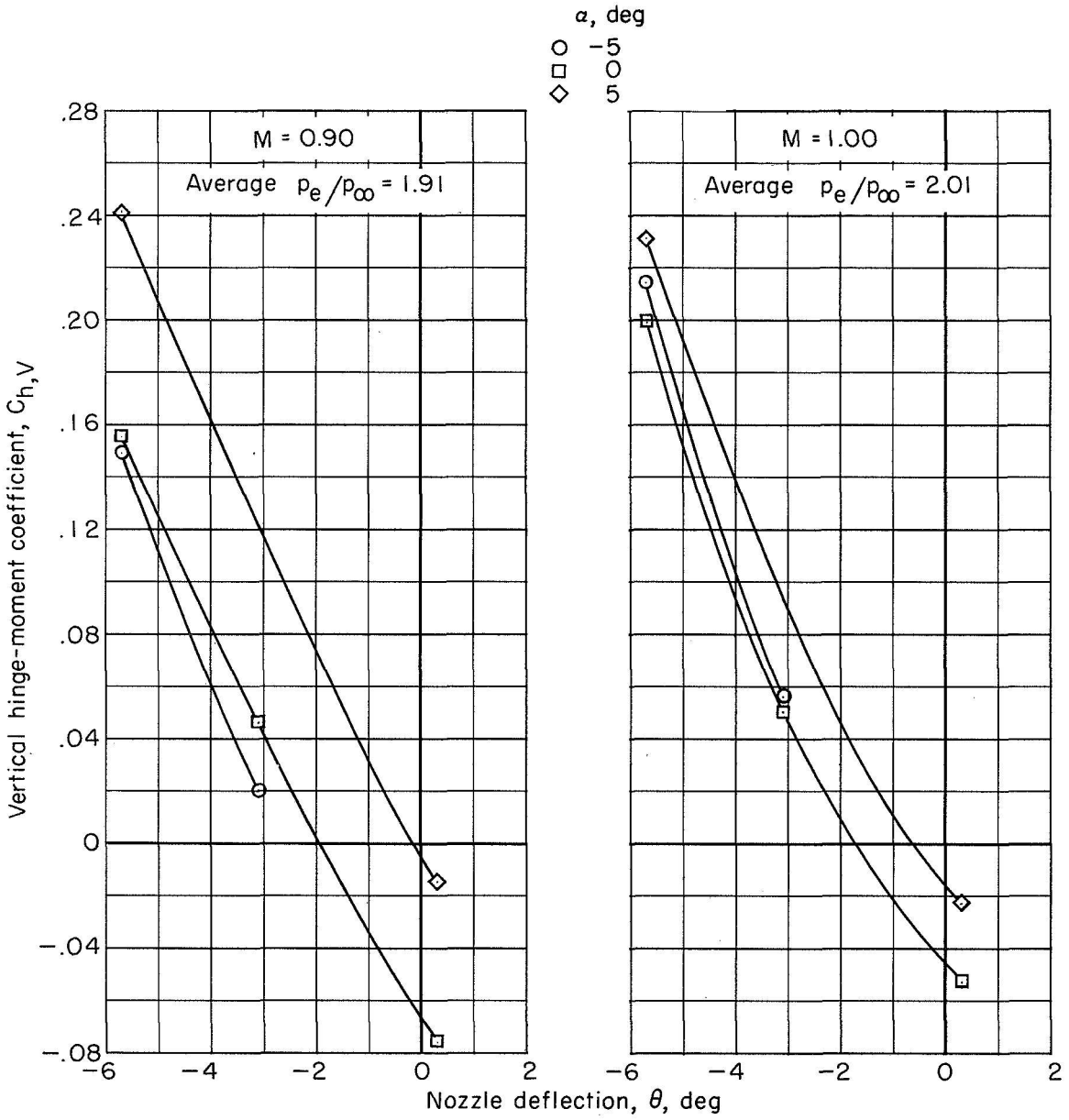

Figure 19.- Variation of vertical hinge-moment coefficient with nozzle deflection. Upper nozzle; basic model; jets on; $\delta = 0^{\circ}$.

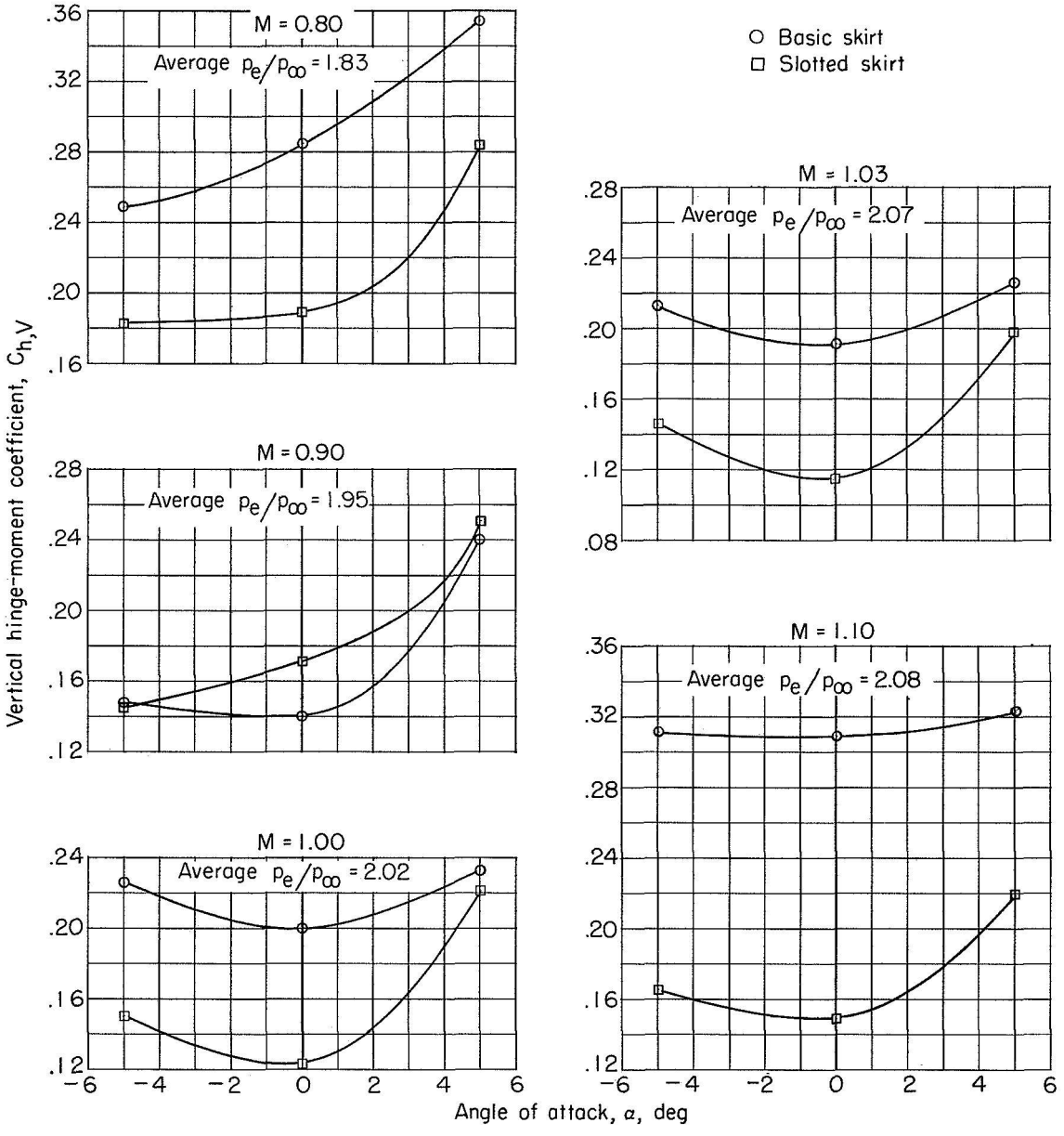

Figure 20.- Effect of slotted skirt on vertical hinge-moment coefficient. $\theta = -5.7^\circ$; $\delta = 0^\circ$; jets on.

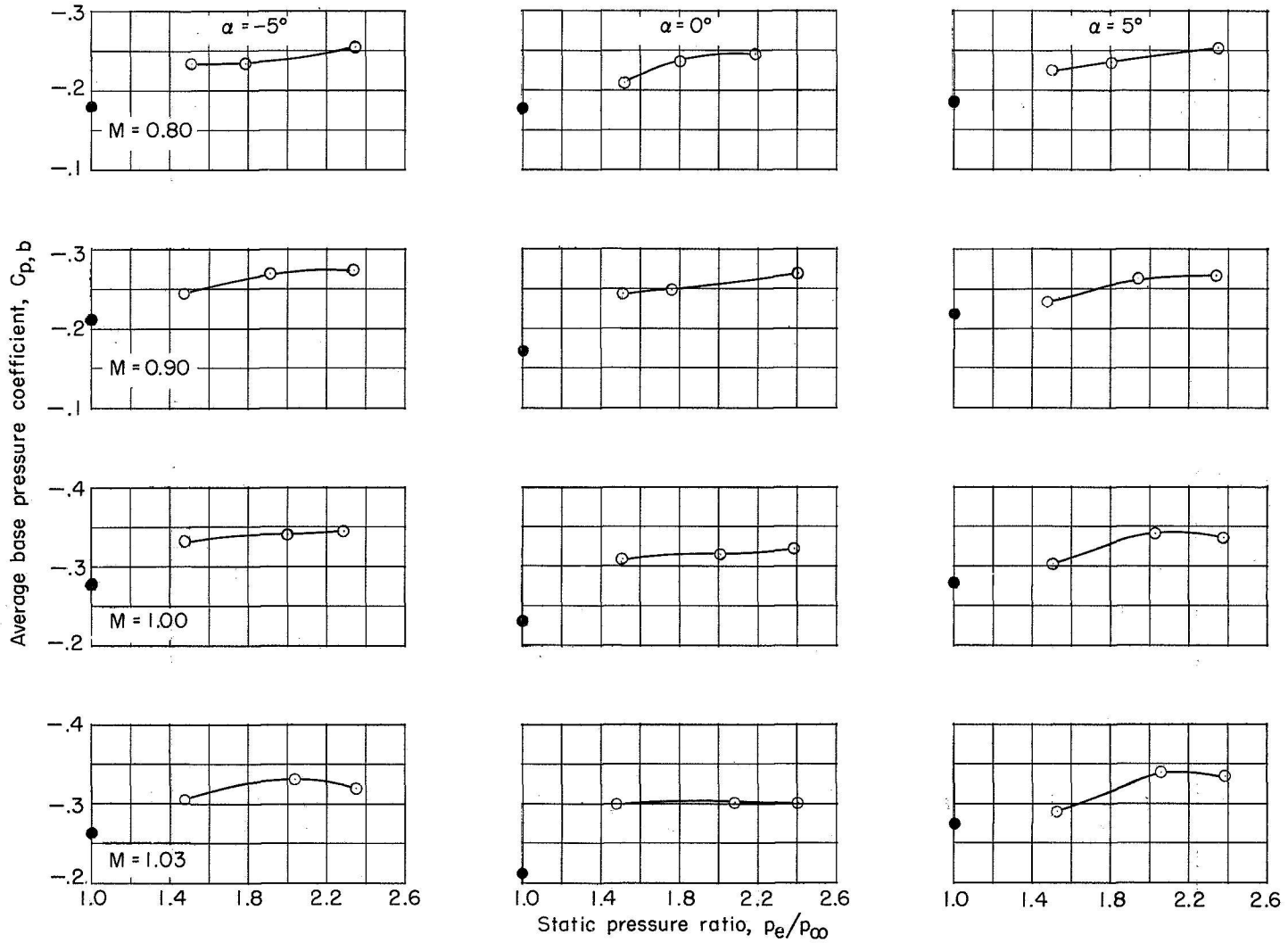

Figure 21.- Variation of average base pressure coefficient with static-pressure ratio. Basic model; $\theta = -5.7^\circ$; $\delta = 0^\circ$. Solid symbols indicate jet off.

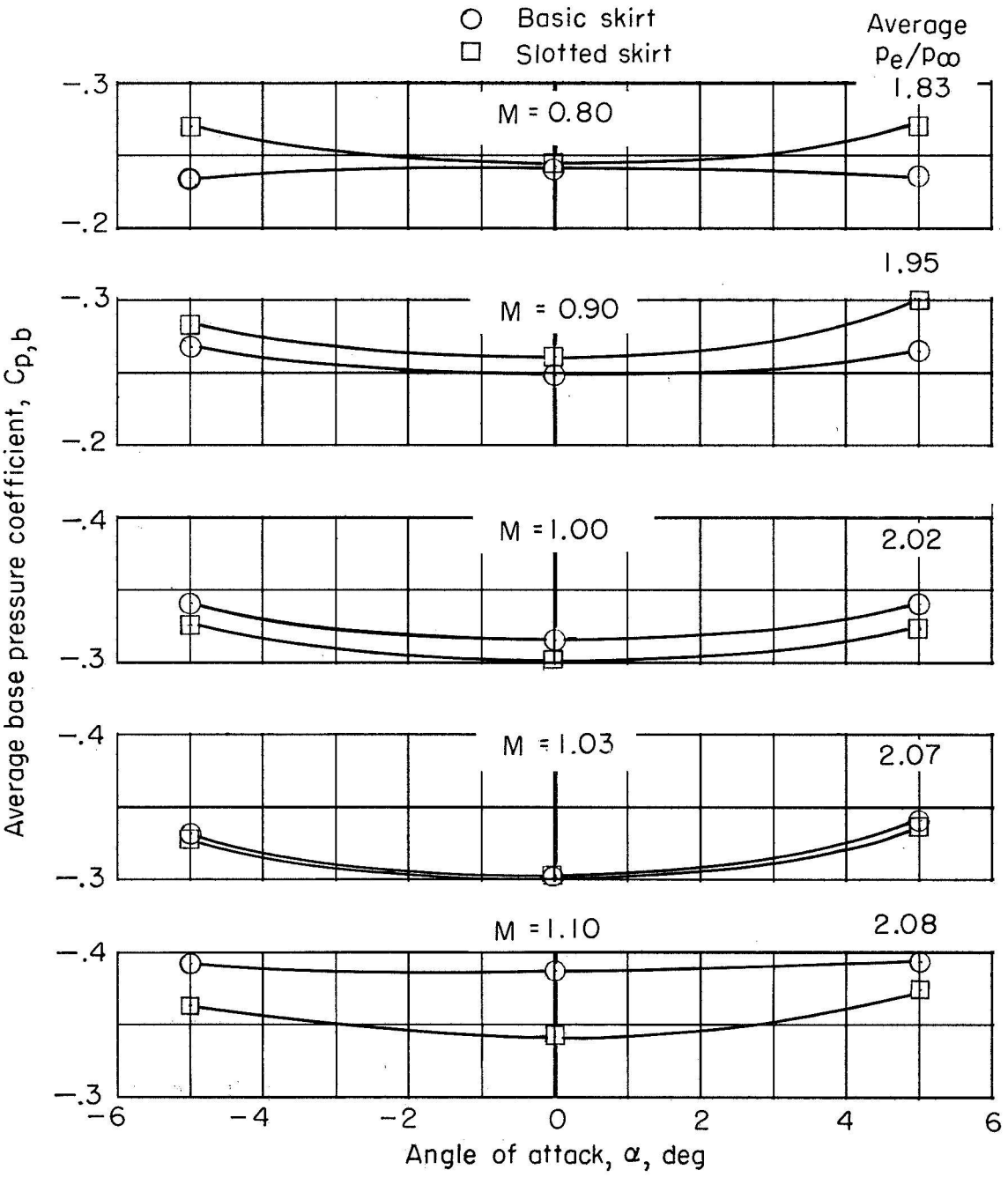

Figure 22.- Effect of slotted skirt on average base pressure coefficient. Jets on; $\theta = -5.7^\circ$; $\delta = 0^\circ$.

L-423

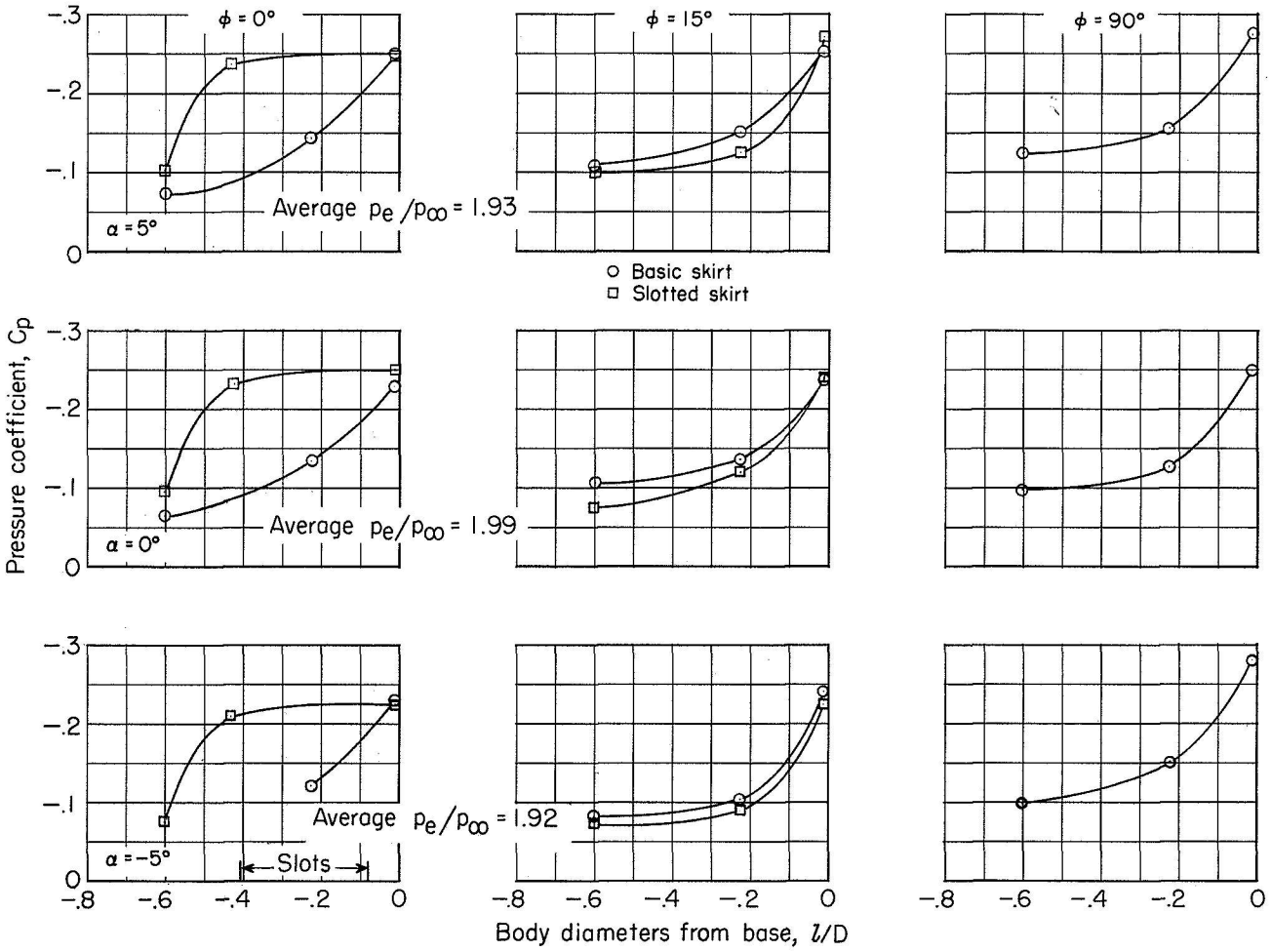

(a) M = 0.90.

Figure 23.- Pressure distributions on skirt for basic- and slotted-skirt configurations. Jets on; $\theta = -5.7^\circ$; $\delta = 0^\circ$.

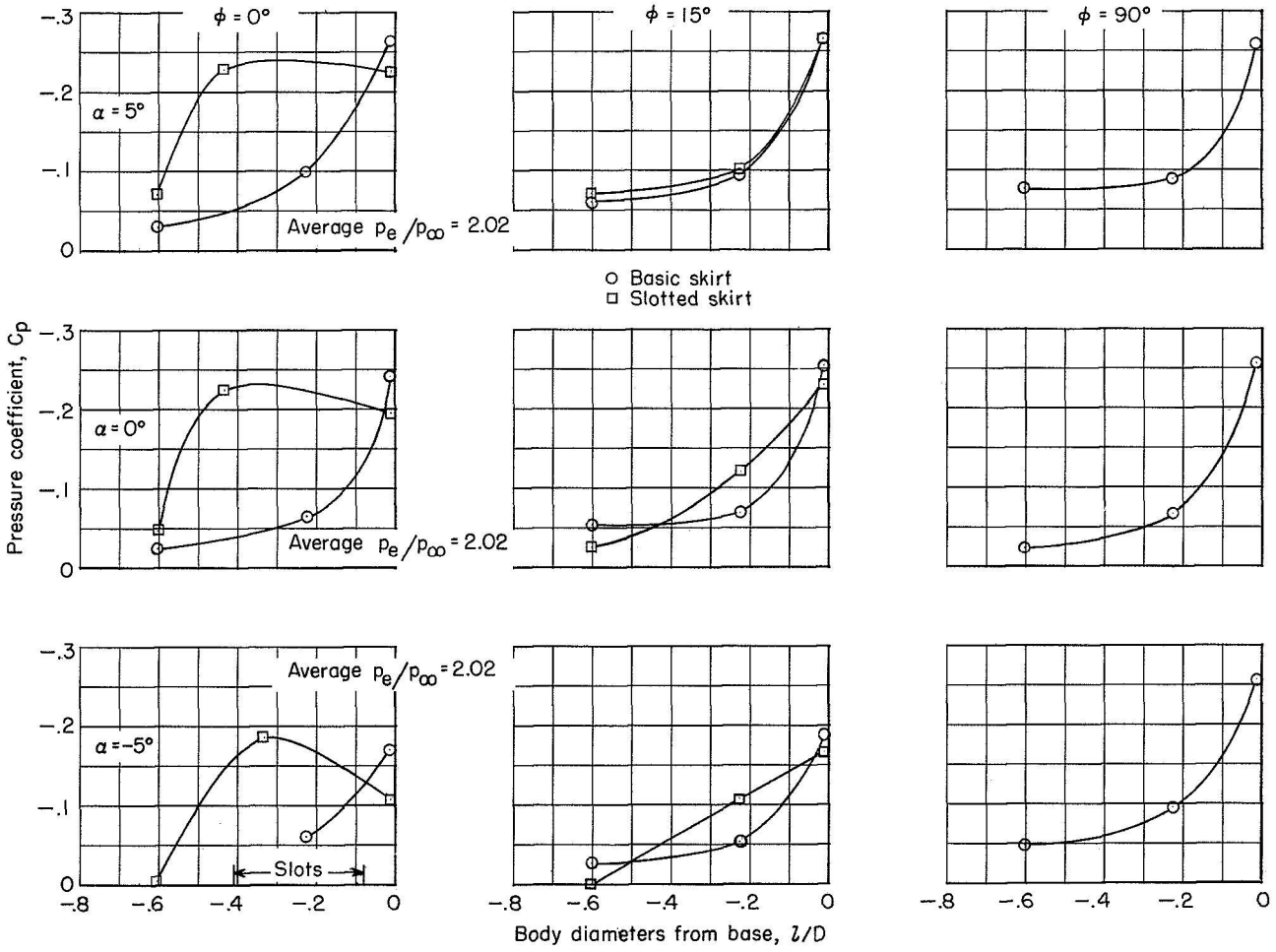

(b) M = 1.00.

Figure 23.- Continued.

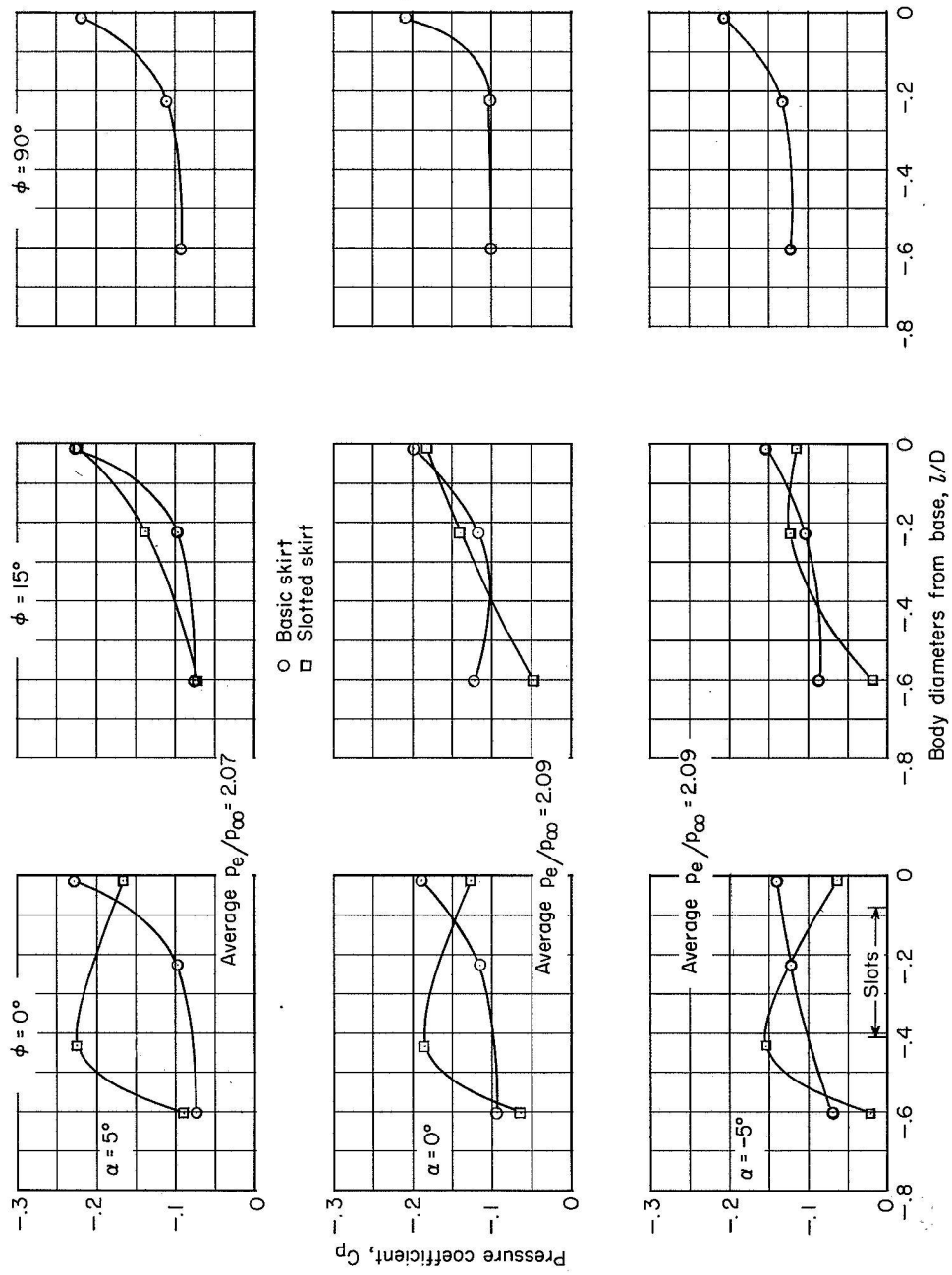

(c) M = 1.10.

Figure 23.- Concluded.

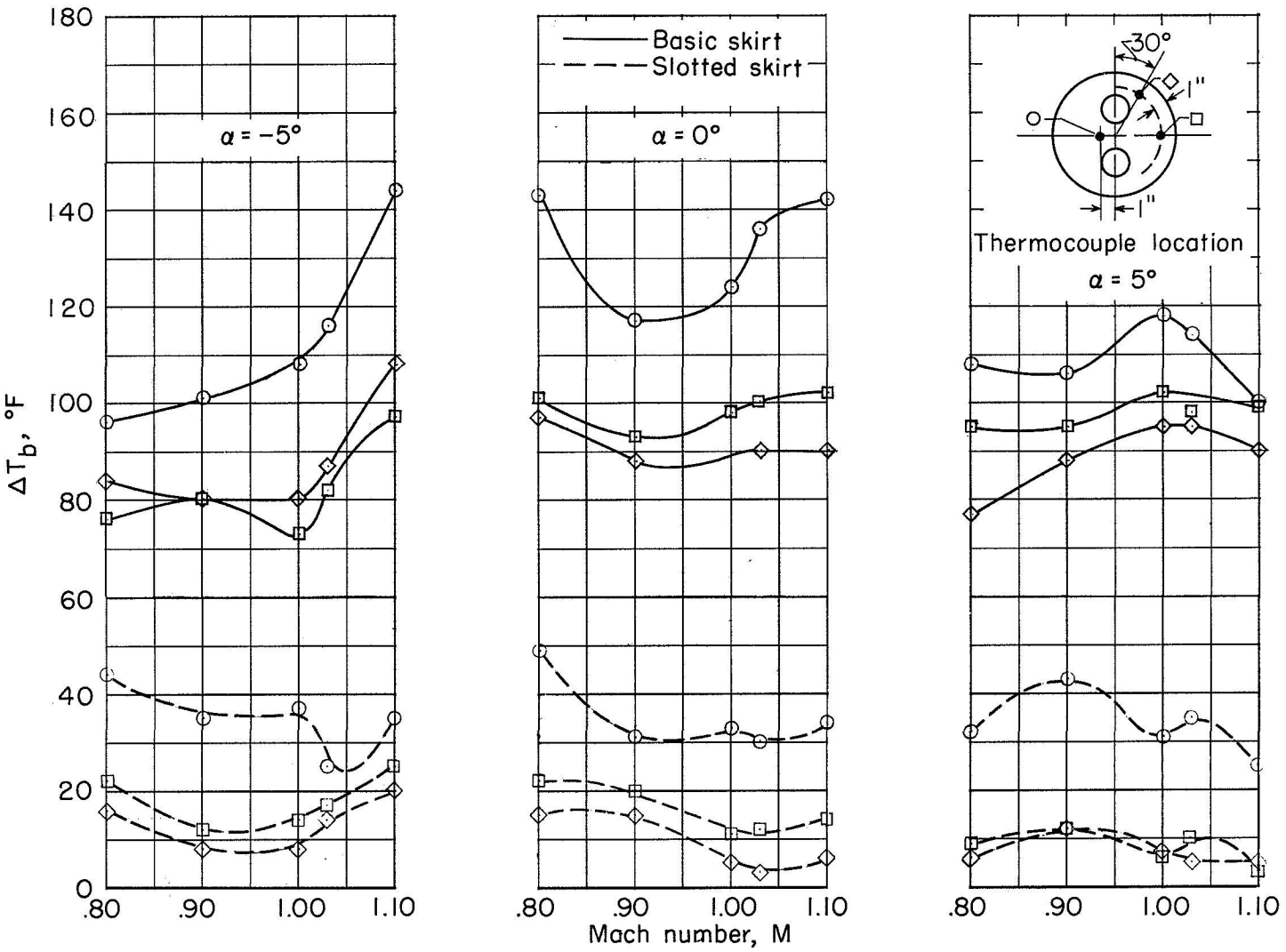

Figure 24.- Effect of slotted skirt on base temperatures. $\Delta T_b = T_{on} - T_{off}$; $\theta = -5.7^\circ$; $\delta = 0^\circ$; scheduled pressure ratio.

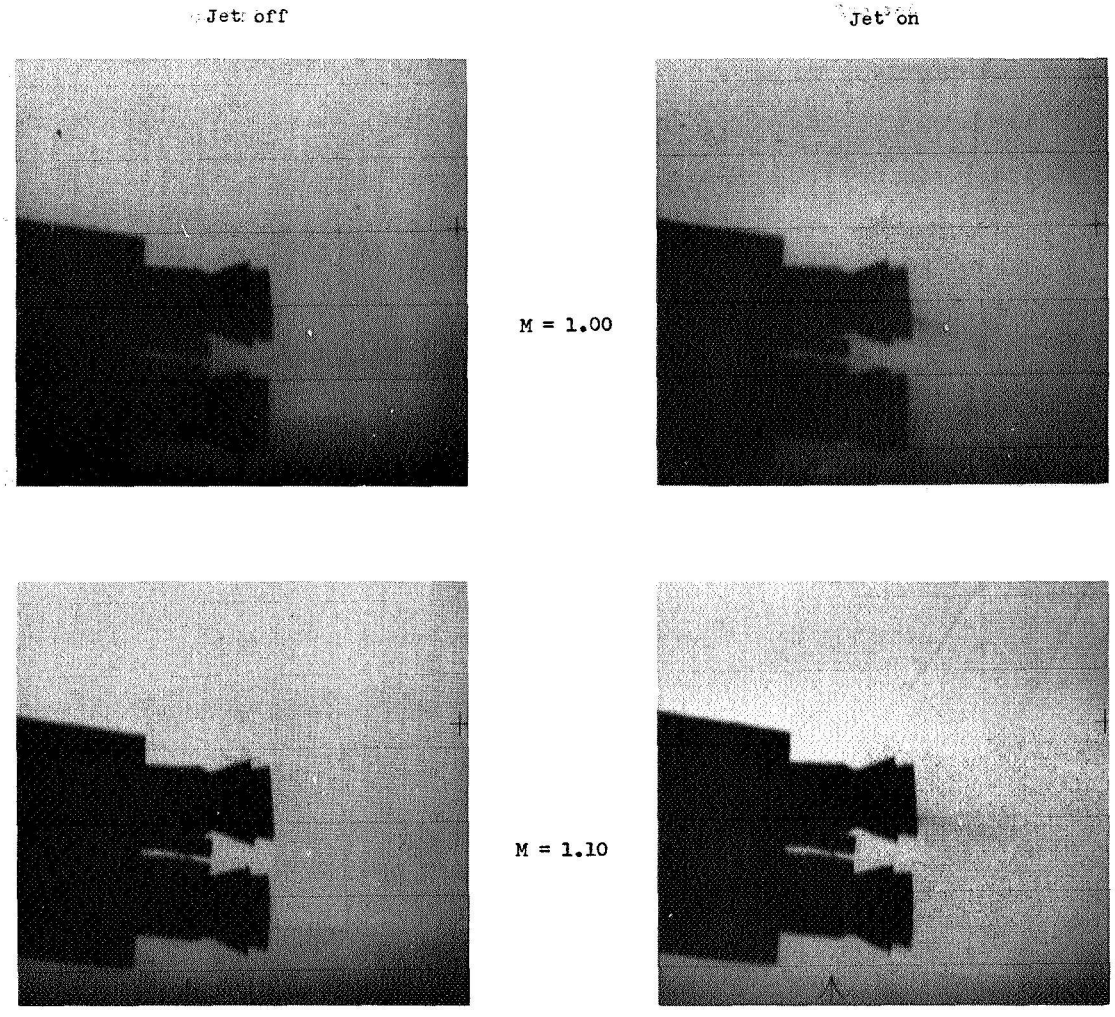

(a) $\alpha = 5^{\circ}$.

L-59-3041

Figure 25.- Shadowgraphs of model. Jets off and jets on; basic skirt; altered nozzles; $\theta = -5.7^{\circ}$; $\delta = 0^{\circ}$.

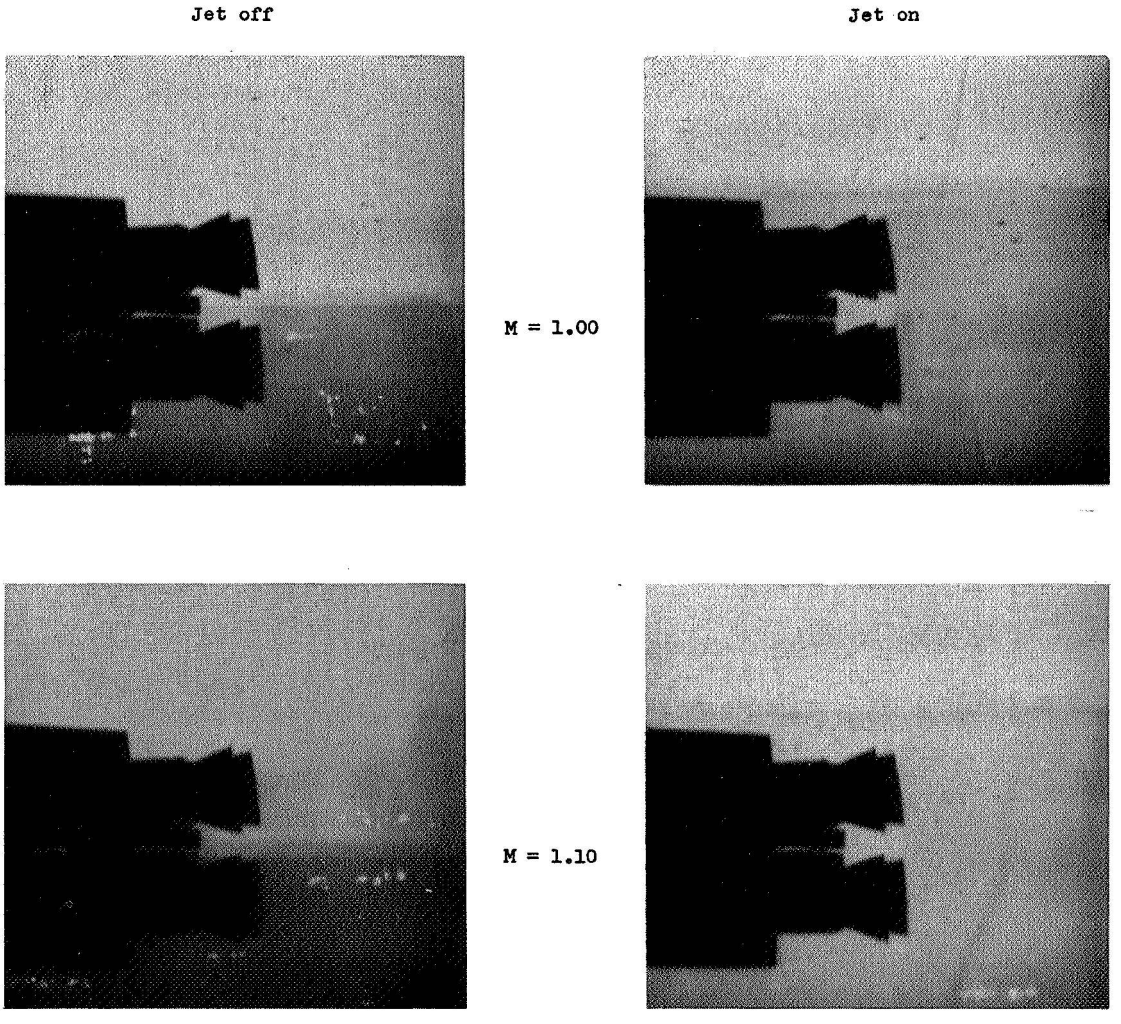

(b) $\alpha = 0^{\circ}$. L-59-3042

Figure 25.- Continued.

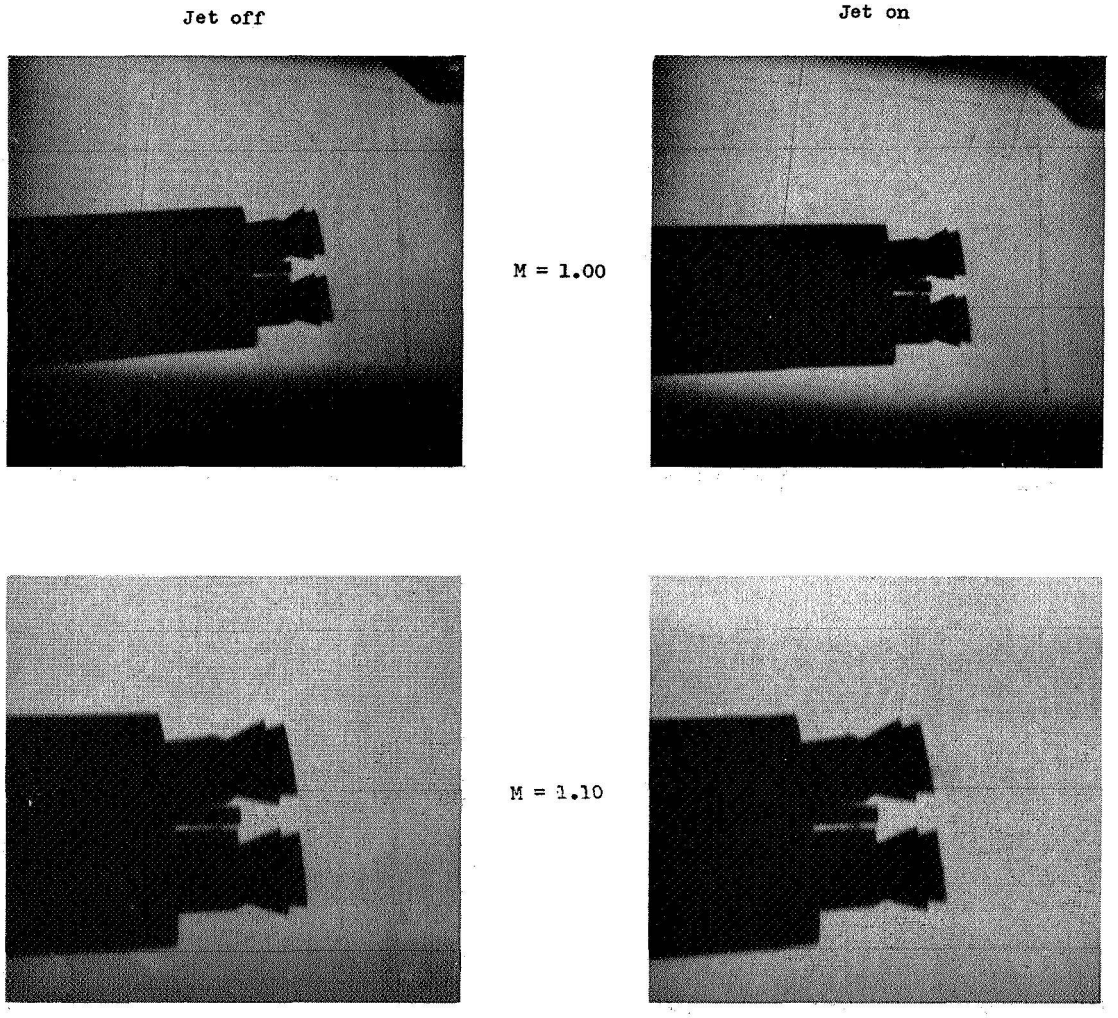

(c) $\alpha = -5^{\circ}$. L-59-3043

Figure 25.- Concluded.

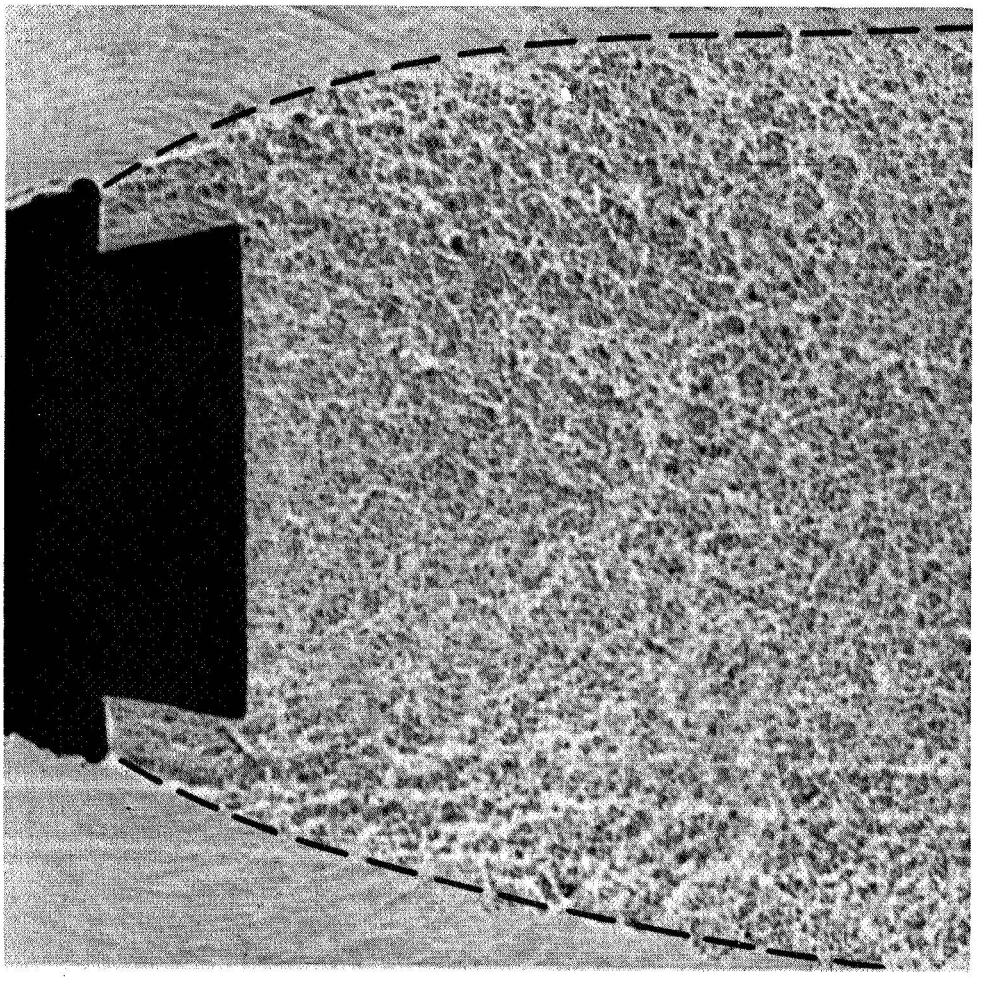

L-423

L-59-3044

Figure 26.- Shadowgraph showing jet boundary. $p_e/p_\infty = 2.05$.

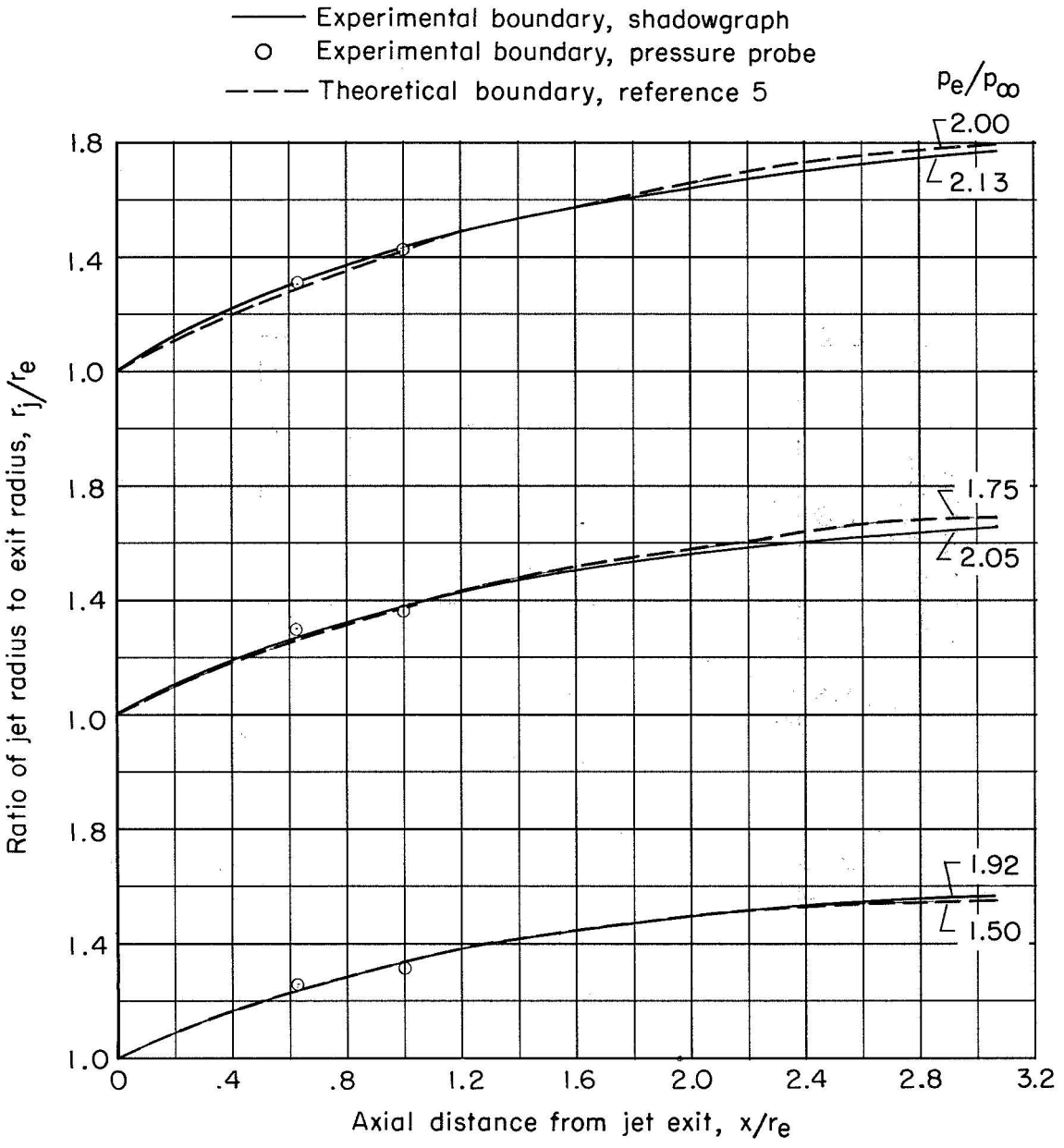

Figure 27.- Comparison of experimental jet boundaries (using flared plug) and theoretical jet boundaries (no plug).

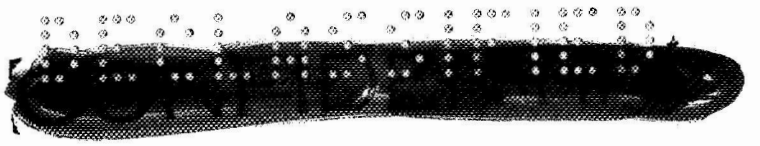

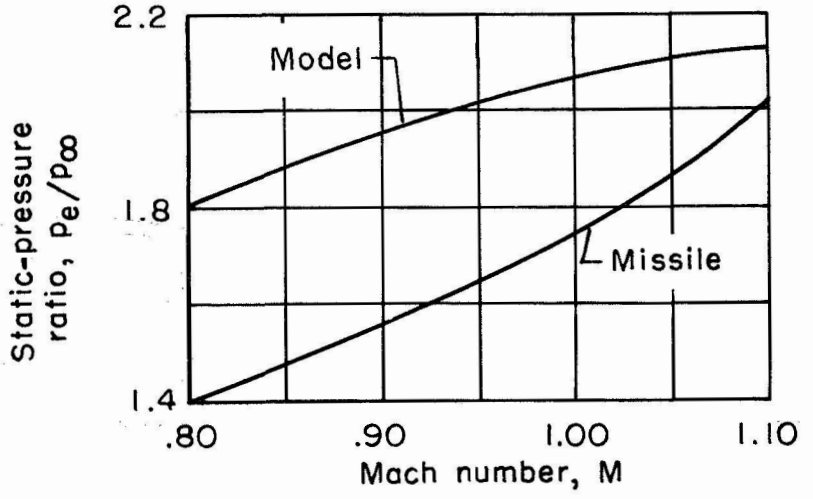

Figure 28.- Nominal-static-pressure-ratio schedule for boundary simulation as determined by static tests.